AGU ADVANCING EARTH AND SPACE SCIENCE

Water Resources Research

RESEARCH ARTICLE
10.1029/2022WR032856

Modified Factorized Transient Wave Model in Tree Pipe Networks for Leak Localization With Less Boundary Measurements

Tong-Chuan Che[1], Xun Wang[2], Ling Zhou[1], and Huan-Feng Duan[3]

[1]College of Water Conservancy and Hydropower Engineering, Hohai University, Nanjing, PR China, [2]School of Reliability and Systems Engineering, Beihang University, Beijing, PR China, [3]Department of Civil and Environmental Engineering, The Hong Kong Polytechnic University, Hong Kong SAR, PR China

Key Points:

- A modified transient wave model is formulated in a general tree pipe network, where the leak location and size are factorized
- An efficient and robust leak localization method can be implemented without the strict accessibility requirements of all boundary pipes
- Numerical and laboratory experiments confirm that a leak anywhere in a tree network can be localized accurately by the proposed algorithm

Correspondence to:

L. Zhou,
zlhhu@hhu.edu.cn

Citation:

Che, T.-C., Wang, X., Zhou, L., & Duan, H.-F. (2022). Modified factorized transient wave model in tree pipe networks for leak localization with less boundary measurements. *Water Resources Research*, *58*, e2022WR032856. https://doi.org/10.1029/2022WR032856

Received 20 MAY 2022
Accepted 14 NOV 2022

Author Contributions:

Conceptualization: Tong-Chuan Che
Formal analysis: Tong-Chuan Che
Funding acquisition: Xun Wang, Ling Zhou, Huan-Feng Duan
Methodology: Tong-Chuan Che, Xun Wang, Ling Zhou
Software: Tong-Chuan Che, Xun Wang
Validation: Tong-Chuan Che
Writing – original draft: Tong-Chuan Che
Writing – review & editing: Tong-Chuan Che, Xun Wang, Ling Zhou, Huan-Feng Duan

Abstract Pressure measurement within each boundary pipe of a tree network has been the prerequisite to the formulation of its factorized transient wave propagation model, which is essential for developing a robust and efficient leak localization algorithm. However, the accessibility of all boundary pipes cannot be always guaranteed in underground pipe networks. The inaccessibility of any one boundary pipe for pressure sensor placement would result in the complete invalidity of this elegant algorithm. To address this problem, this paper reformulates and modifies the factorized wave propagation model, which allows the leak localization algorithm to be implemented without the strict accessibility requirement of all boundary pipes. This is realized by linearizing and factorizing the point transfer matrices of boundary pipes based on the small leak approximation. Numerical experiments demonstrate that the modified algorithm can accurately localize a single leak and give a good estimation of multiple co-existing leaks in a tree network. Moreover, the modified algorithm is verified by recent laboratory experiments conducted in a tree network of viscoelastic pipes, where a leak is successfully localized.

1. Introduction

In the United States (US), the total length of water mains is around 2 million kilometers (i.e., 50 times the equatorial circumference), most of which have been buried underground over half a century (Che et al., 2021). Due to aging without timely and effective renewal, a large portion of these pipes have reached or are reaching the end of their service lives. The quality of service to water users has been significantly going down in recent decades because of the occurring leaks in urban water supply systems (Alawadhi et al., 2018). It was estimated that the annual loss of drinking water worldwide is 126 billion m^3 (i.e., about 70 L per person per day), at a direct cost of US$39 billion, mostly from hidden leaks (Liemberger & Wyatt, 2019). Moreover, external contaminants can be easily drawn into the pipe system via leaks under low internal pressure conditions, which poses a serious threat to public health (Alawadhi & Tartakovsky, 2020; Fernandes & Karney, 2004; Huang et al., 2020; Qi et al., 2018). The existing commercialized leak localization techniques have made a valuable contribution toward the conservation of water resources (Hamilton & Charalambous, 2013), but the severe situation of water and energy loss also indirectly indicates the inefficiency and insufficiency of most existing techniques. Therefore, it is urgent and crucial to develop a more efficient and comprehensive leak localization method for such a large-scale pipe system.

A leak localization method should, ideally, be accurate, efficient, cost-effective, and not disturb the normal supply to water users. The emerging transient wave-based leak localization method potentially fulfills these requirements of water operators (Che et al., 2021; Colombo et al., 2009; Duan et al., 2020). The basic idea of this method is to actively send a transient pressure wave (hereinafter called transient wave or pressure wave) into the target pipe system by a fast flow change (e.g., via valve closure). The sent pressure wave travels in the water of the pipe, with a high propagating speed (e.g., around 1,000 m/s in elastic pipes and 300 m/s in viscoelastic pipes), interacts and reflects when it meets any pipe defect (e.g., leak, partial blockage, or wall corrosion). The reflections are the response of the pipe system to the sent wave, which carry physical information of leak parameters (i.e., location and size). Therefore, based on the measured pressure response, the leak in water pipes can be localized using wave physics and signal processing techniques (Meniconi et al., 2015). The feasibility of the transient wave-based method has been confirmed, with quite promising results, in real branched transmission mains which are usually used to convey water from treatment plants to service reservoirs (Meniconi, Capponi, et al., 2021). The real water distribution networks, which supply water from the service reservoirs to consumers, are still challenging systems

for the transient wave-based method because of the existence of a great deal of complexities and uncertainties (Meniconi et al., 2015).

From a perspective of inverse problem, the transient wave-based method consists of two main categories: (i) local feature-based method, and (ii) full-waveform inversion (FWI) method (Che et al., 2021; Wang et al., 2021). The local feature-based method only utilizes partial leak-induced information (e.g., reflection, damping, or resonant peaks) for localization, which includes three sub-categories: (i-a) reflection-based method (Brunone, 1999; Ferrante & Brunone, 2003; Ferrante et al., 2007; Lee et al., 2007; Meniconi, Capponi, et al., 2021; Zeng et al., 2020), (i-b) damping-based method (Capponi et al., 2020; Nixon et al., 2006; Wang et al., 2002), and (i-c) frequency response function (FRF) peak pattern-based method (Duan, 2017; Gong et al., 2013; Lee et al., 2006). Whereas the FWI method uses the entire measured pressure response for leak localization, which are further classified into two sub-categories: (ii-a) time domain FWI method (Covas & Ramos, 2010; Kapelan et al., 2003; Kim et al., 2014; Liggett & Chen, 1994), and (ii-b) frequency domain FWI method (Che et al., 2022; Keramat et al., 2021; Wang & Ghidaoui, 2018a, 2018b; Wang et al., 2021). In addition to above model-based methods, several recent studies (Bohorquez et al., 2020, 2022) have also preliminarily demonstrated the potential of the machine learning-based method for leak localization using pressure waves, which is purely data-driven but needs large amounts of practical data for training.

Although most of the above transient wave-based methods are mainly developed for leak localization in single pipes, they have also been extended to tree pipe networks (hereinafter called tree networks) (Meniconi, Cifrodelli, et al., 2021). Specifically, the reflection-based method estimates the distance between the potential leak and the sensor based on the known wave speed and arriving time of the first leak-induced reflection (Beck et al., 2005; Ferrante et al., 2009; Nguyen et al., 2018). However, the exact leak location cannot be uniquely determined due to the multiple possible wave propagation paths in a tree network corresponding to the same arriving time. Moreover, the reflection-based method only uses information of the first reflection, which is a short-time (local) feature, instead of a long-time (global) feature; thus, it can be easily contaminated by background noise. The FRF peak pattern-based method utilizes the leak-induced pattern on FRF resonant peaks to localize a leak (Duan, 2017; Pan et al., 2022). Since only the information at resonant frequencies, instead of all frequencies, is used, this method is also not robust to noise. In addition, the theoretical derivation of the leak-induced pattern is a long and laborious process, whose complexity increases significantly with the network complexity. The time domain FWI method estimates unknown leak parameters by matching the measured signal with numerically simulated signals (Liggett & Chen, 1994). This method is relatively robust to noise compared with the previous two methods, because it uses the full measured information. However, it needs to solve a nonlinear high-dimensional optimization problem, which converges slowly and is easily trapped into local optimums. The heavy burden on numerical computations of the time domain FWI method was partially reduced by Capponi et al. (2017) and Kim (2016), where the simulated signals are computed analytically by the frequency domain model. Nonetheless it is still a nonlinear high-dimensional optimization problem and the influence of noise is neglected.

The urban water supply systems are complicated and full of natural and artificial noise (e.g., turbulence and traffic) (Alawadhi & Tartakovsky, 2020; Lin et al., 2021; Wang, 2021; Waqar et al., 2021). To address the above-mentioned noise problem of the reflection-based, FRF peak pattern-based, and time domain FWI methods, Wang et al. (2021) proposed a leak localization method for tree networks using the matched-field processing (MFP) technique, which is essentially one of the (ii-b) frequency domain FWI methods. MFP is a parameter estimation technique that is based on the principle of maximum signal-to-noise ratio (SNR); thus, it is robust in noisy and uncertain environments. A factorized transient wave model (hereinafter called factorized wave model), where the leak parameters are decoupled, allows the MFP method to estimate the leak location and size separately and sequentially. Therefore, this method is efficient, accurate, and provides a unique leak location. The formulation of the factorized wave model and implementation of the MFP method need to place one pressure sensor in each boundary pipe of a buried tree network. This makes the existing MFP method be a zero-tolerance approach against inaccessibility of any boundary pipe. However, the accessibility of all boundary pipes is often unrealistic for underground networks, which limits the application of the MFP method in real urban water supply systems.

To address this problem, this paper reformulates the MFP method for leak localization based on a modified factorized wave model, where the tolerance for inaccessibility of boundary pipes is largely improved. Specifically, Section 2 presents the modified factorized wave model in a general tree network, based on which the MFP method is reformulated in Section 3. The validity of the modified factorized wave model is first confirmed by

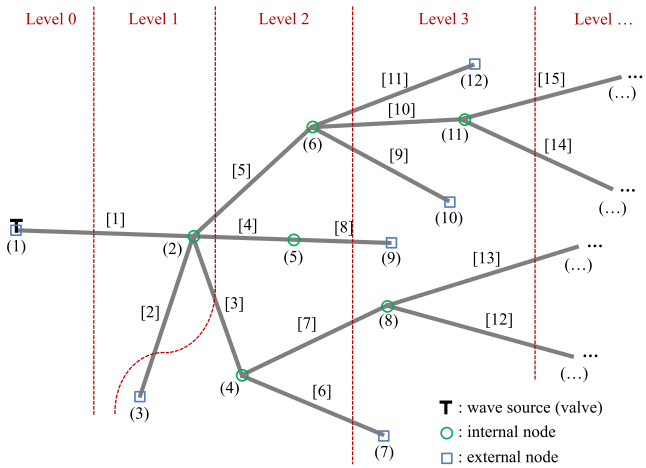

Figure 1. Graph of a general tree network.

numerical experiments in Section 4. Finally, a leak is successfully localized by the reformulated MFP method using laboratory data contaminated by noise in Section 5. Main conclusions are drawn in Section 6.

2. Modified Factorized Transient Wave Model for Tree Networks

This section introduces both the original and modified factorized wave models for tree networks with a leak. To facilitate the understanding, the properties and wave models of a general tree network are first given, which are subsequently illustrated by specific examples of a simple tree network.

2.1. Nomenclature of Tree Networks

This sub-section introduces the basic concepts and properties of tree networks, which will be used in the rest of this paper. Note that pipe networks with loops are out of the main scope of this paper. Fortunately, well-designed pipe systems are usually equipped with sufficient isolating valves, where a looped network can be ideally isolated into a tree network (Wang et al., 2021).

Figure 1 shows the graph of a general tree network. To clearly describe the network components and properties, a tree network is represented by a connected graph $T(V, E)$ (Che et al., 2022; Zecchin et al., 2014), which includes the node set (i.e., all vertexes) $V = \{(v_1), (v_2), \ldots, (v_N)\}$ and the pipe set (i.e., all edges) $E = \{[e_1], [e_2], \ldots, [e_P]\}$, where v_n = ID number of the nth node in V and e_p = ID number of the pth pipe in E. Node set V can be further classified according to the direct connectivity of a node with boundaries (e.g., reservoirs, valves, and dead ends) - that is *internal node* set V_{in}, where different pipe ends meet, and *external node* set V_{ex}, where a pipe connects to a boundary, such that $V = V_{in} \cup V_{ex}$, where $\cup$ = union operator (Karney & McInnis, 1992). An external node links only one pipe, whereas an internal node connects at least two pipes. A wave source (e.g., a valve) is usually placed at an access point of one external node to generate pressure waves. Different types of wave generator and their features were previously reviewed and summarized by Brunone et al. (2022) and Che et al. (2021). The node with the wave source is termed V_s. The total number of nodes is expressed as $N = |V| = N_{in} + N_{ex} \in \mathbb{N}^+$, where $N_{in} = |V_{in}|$ = the number of internal nodes and $N_{ex} = |V_{ex}|$ = the number of external nodes. All nodes are classified into different *levels*, where the wave source is located at Level 0. Each pipe links two nodes in neighbor levels, where the *upstream* and *downstream ends* of Pipe $[p]$ connects with higher and lower levels, whose local coordinates are x_p^U and x_p^D, respectively. Each internal node at Level l links with: (i) the node at lower Level $l-1$ by its unique *mother pipe*, and (ii) nodes at higher Level $l+1$ by its I_c *child pipes*, where I_c = the total number of its child pipes. Likewise, pipe set E is also classified into two subsets: *internal pipe* set E_{in}, where each pipe is bounded by two internal nodes, and *external pipe* set E_{ex}, where one end of each pipe is connect with an external node, such that $E = E_{in} \cup E_{ex}$. $P = |E| \in \mathbb{N}^+$ is the total number of pipes. A *path* is defined as the pipe set $R_{v_0,v_E} = \{[e_1], [e_2], \ldots, [e_K]\}$ between two nodes v_0 and v_E, where v_0 = the starting node, v_E = the end node, e_k = ID number of the kth pipe in R_{v_0,v_E}, and $K = |R_{v_0,v_E}|$ is the total number of pipes along this path. In a tree network, there is a unique path between any two different nodes.

Example 1. A simple tree network in Figure 2 is used to illustrate the above nomenclature. This tree network $T(V, E)$ consists of the node set $V = \{(1), (2), (3), (4)\}$ and the pipe set $E = \{[1], [2], [3]\}$. The total number of nodes is $N = |V| = N_{in} + N_{ex} = 4$, in which $N_{in} = |V_{in}| = 1$, namely Node (2), and $N_{ex} = |V_{ex}| = 3$, namely Nodes (1), (3) and (4). The valve at Node (3) is the wave source, that is, $V_s = \{(3)\}$. Nodes (1) and (4) are connected to a constant-head reservoir and a dead end, respectively. All nodes in Figure 2 are classified into three levels, that is, Level 0, Level 1, and Level 2. The local coordinates of upstream and downstream ends of Pipe [2], which connect with Node (2) at Level 1 and Node (3) at Level 0, are x_2^U and x_2^D, respectively. Internal Node (2) has its unique mother pipe (i.e., Pipe [2]) and two child pipes (i.e., Pipe [1] and Pipe [3]). The total number of pipes is $P = |E| = 3$, which are all external pipes since one end of each pipe is connected to an external node. There is a unique path, that is, $R_{1,3} = \{[1], [2]\}$, between Node (1) and Node (3).

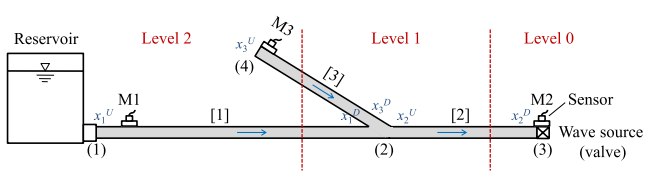

Figure 2. Graph of a simple tree network with three pipes.

2.2. Wave Propagation Model for Single Pipes

This sub-section introduces the wave propagation model for single pipes, which is the basis for the wave propagation models of tree networks in the next two sub-sections, that is, Sections 2.3 and 2.4.

In Pipe [p] of a tree network, the transient state hydraulic properties (i.e., discharge q and pressure head h) of its upstream and downstream ends at a specific frequency can be connected by a 2×2 filed transfer matrix $\mathbf{F}$ as (Chaudhry, 2014; Wang & Ghidaoui, 2018b)

$$\begin{bmatrix} q\left(x_p^D\right) \\ h\left(x_p^D\right) \end{bmatrix} = \mathbf{F}\left(x_p^U \to x_p^D\right) \begin{bmatrix} q\left(x_p^U\right) \\ h\left(x_p^U\right) \end{bmatrix} \tag{1}$$

where q = discharge perturbation from the mean in the frequency domain; h = pressure head perturbation from the mean in the frequency domain; and $\mathbf{F}\left(x_p^U \to x_p^D\right)$ = field transfer matrix (hereinafter called field matrix) depicting the wave propagation from x_p^U to x_p^D. Note that Equation 1 represents the mass and momentum equations in the frequency domain.

When there is no physical discontinuity (i.e., leak in this paper) in Pipe [p], its field matrix $\mathbf{F}\left(x_p^U \to x_p^D\right)$ in Equation 1 can be written as (Chaudhry, 2014)

$$\mathbf{F}^{NL}\left(x_p^U \to x_p^D\right) = \begin{bmatrix} F_{11}(L_p) & F_{12}(L_p) \\ F_{21}(L_p) & F_{22}(L_p) \end{bmatrix} = \begin{bmatrix} \cosh(\mu L_p) & -\frac{1}{Z}\sinh(\mu L_p) \\ -Z\sinh(\mu L_p) & \cosh(\mu L_p) \end{bmatrix} \tag{2}$$

where the superscript "NL" means no leak; F_{ij} = an element in row i and column j of $\mathbf{F}^{NL}$, in which $i, j = 1$ or 2; L_p = length of Pipe [p]; $Z = \mu a^2/i\omega gA$ is the characteristic impedance; $\mu = \sqrt{-\omega^2 + igA\omega R}/a$; and $R = f_{DW}Q_0/gDA^2$ is the resistance term for turbulent pipe flows; in which $i = \sqrt{-1}$, a = wave speed, ω = angular frequency, g = gravitational acceleration, A = pipe cross-sectional area, f_{DW} = Darcy–Weisbach friction factor, Q_0 = steady state discharge, and D = pipe diameter.

When there is a leak in Pipe [p^L], Wang and Ghidaoui (2018b) proved that its field matrix $\mathbf{F}\left(x_p^U \to x_p^D\right)$ in Equation 1 can be expressed as

$$\mathbf{F}^{WL}\left(x_p^U \to x_p^D\right) = \mathbf{F}^{NL}\left(x_p^U \to x_p^D\right) + s_p^L \mathbf{F}^{SL}\left(x_p^U \to x_p^L \to x_p^D\right) \tag{3}$$

where superscript "WL" means with leak; s_p^L = leak size; x_p^L = leak location; p^L = ID number of the leaky pipe; and $\mathbf{F}^{SL}$ = scattering matrix due to leak can be expressed as

$$\begin{aligned} \mathbf{F}^{SL}\left(x_p^U \to x_p^L \to x_p^D\right) &= \begin{bmatrix} F_{11}^{SL}\left(x_p^L\right) & F_{12}^{SL}\left(x_p^L\right) \\ F_{21}^{SL}\left(x_p^L\right) & F_{22}^{SL}\left(x_p^L\right) \end{bmatrix} \\ &= \sqrt{\frac{g}{2H_0^L}} \begin{bmatrix} Z\cosh\left[\mu\left(x_p^D - x_p^L\right)\right]\sinh\left[\mu\left(x_p^L - x_p^U\right)\right] & -\cosh\left[\mu\left(x_p^D - x_p^L\right)\right]\cosh\left[\mu\left(x_p^L - x_p^U\right)\right] \\ -Z^2\sinh\left[\mu\left(x_p^D - x_p^L\right)\right]\sinh\left[\mu\left(x_p^L - x_p^U\right)\right] & Z\sinh\left[\mu\left(x_p^D - x_p^L\right)\right]\cosh\left[\mu\left(x_p^L - x_p^U\right)\right] \end{bmatrix} \end{aligned} \tag{4}$$

in which F_{ij}^{SL} = an element in row i and column j of $\mathbf{F}^{SL}(i, j = 1$ or 2), and H_0^L = steady state pressure head at the leak.

As a result, the field matrix $\mathbf{F}^{WL}$ of the pipe with a leak is decomposed into a field matrix $\mathbf{F}^{NL}$ independent of leak parameters and the leak size s_p^L times a scattering matrix $\mathbf{F}^{SL}$ dependent on the leak location x_p^L.

2.3. Original Factorized Transient Wave Model for Tree Networks

This sub-section introduces the original factorized wave model for tree networks with a leak proposed by Wang et al. (2021) and its problem in the application, which will be modified and fixed in the next sub-section, that is, Section 2.4.

In a general tree network, as introduced in Section 2.1, there is a unique path between any external node except the wave source $V_{ex}\backslash V_s$ and the wave source V_s, where the "\" represents the relative complement. Thus, once the

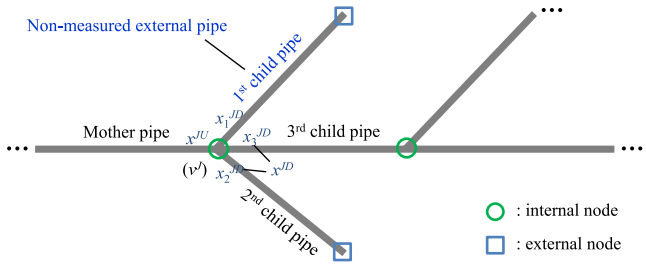

Figure 3. An internal node with its mother pipe and child pipes.

q and h at each external node in $V_{ex}\backslash V_s$ are known (e.g., assumed, measured, or computed), the q and h at the wave source V_s can be represented based on the superposition principle of $V_{ex}\backslash V_s$ by the transfer matrix method (Wang et al., 2021).

Figure 3 shows a general internal Node (v^J) of a tree network, the coordinate of the pipe end in its mother pipe, infinitely close to Node (v^J), is x^{JU}. Similarly, the coordinate of the pipe end in its ith child pipe, infinitely approaching Node (v^J), is expressed as x_i^{JD} $(i = 1, 2, \ldots, I_c)$. Therefore, the mass and momentum equations across the internal Node (v^J) are written as

$$\begin{bmatrix} q(x^{JU}) \\ h(x^{JU}) \end{bmatrix} = \mathbf{P}_{22} \begin{bmatrix} q(x_1^{JD}) \\ h(x_1^{JD}) \end{bmatrix} + \sum_{i=1}^{I_c} (-1)^{\alpha_i} \mathbf{P}_{11} \begin{bmatrix} q(x_i^{JD}) \\ h(x_i^{JD}) \end{bmatrix} \tag{5}$$

where $\mathbf{P}_{ii}$ = a 2×2 point transfer matrix (hereinafter called point matrix) depicting the wave propagation across an internal node, specifically $\mathbf{P}_{11} = \begin{bmatrix} 1 & 0 \\ 0 & 0 \end{bmatrix}$ and $\mathbf{P}_{22} = \begin{bmatrix} 0 & 0 \\ 0 & 1 \end{bmatrix}$; $\alpha_i = 0$ if the discharge in the ith child pipe is in the opposite direction with the mother pipe toward Node (v^J), otherwise $\alpha_i = 1$; and $\sum$ = summation operator. Equation 5 shows that, at an internal node, the discharge of its mother pipe is the summation of all child pipes, whereas the pressure head of the mother pipe only takes the value of the first child pipe.

The wave propagation is computed from $N_{ex} - 1$ external nodes $V_{ex}\backslash V_s$ toward the wave source V_s. The unique path between the nth external node and the wave source covers l_n pipes and $l_n - 1$ internal nodes. Thus, the q and h at the wave source can be represented as

$$\begin{bmatrix} q(x^M) \\ h(x^M) \end{bmatrix} = \sum_{n=1}^{N_{ex}-1} \mathbf{F}\left(x_{n_{l_n}}^U \rightarrow x^M\right) \left[\prod_{j=l_n-1}^{1} \mathbf{P}^{(n_j)} \mathbf{F}\left(x_{n_j}^U \rightarrow x_{n_j}^D\right)\right] \begin{bmatrix} q(x_{n_1}^U) \\ h(x_{n_1}^U) \end{bmatrix} \tag{6}$$

where x^M = pressure sensor coordinate at the wave source; $x_{n_j}^U, x_{n_j}^D$ = coordinates of upstream and downstream ends of the n_j-th pipe between the nth external node and the wave source; $\mathbf{P}^{(n_j)} = \mathbf{P}_{22} + (-1)^{\alpha_{n_j}} \mathbf{P}_{11}$ if n_j is the first child pipe of an internal node at Level l, otherwise $\mathbf{P}^{(n_j)} = (-1)^{\alpha_{n_j}} \mathbf{P}_{11}$; and $\prod$ = product operator.

Equation 6 is a linear superposition-based wave propagation model, which has the desirable attributes of easy factorization, numerical efficiency, and programming simplicity.

When there is no leak in the tree network, Equation 6 becomes

$$\begin{bmatrix} q^{NL}(x^M) \\ h^{NL}(x^M) \end{bmatrix} = \sum_{n=1}^{N_{ex}-1} \mathbf{F}^{NL}\left(x_{n_{l_n}}^U \rightarrow x^M\right) \left[\prod_{j=l_n-1}^{1} \mathbf{P}^{(n_j)} \mathbf{F}^{NL}\left(x_{n_j}^U \rightarrow x_{n_j}^D\right)\right] \begin{bmatrix} q(x_{n_1}^U) \\ h(x_{n_1}^U) \end{bmatrix} \tag{7}$$

When there is a leak in Pipe $[p^L]$, its transfer matrix is in the form of Equation 3. Substituting Equation 3 into Equation 6 results in

$$\begin{bmatrix} q(x^M) \\ h(x^M) \end{bmatrix} = \begin{bmatrix} q^{NL}(x^M) \\ h^{NL}(x^M) \end{bmatrix} + s_p^L \begin{bmatrix} q^*(x^M, x_p^L) \\ G(x^M, x_p^L) \end{bmatrix} \tag{8}$$

where q^* and G = functions of the leak location x_p^L, which are independent of the leak size s_p^L. Their detailed forms depend on the leak location and topological structure of the pipe network.

The second row of Equation 8 gives the measured pressure head at x^M as

$$h(x^M) = h^{NL}(x^M) + s_p^L G(x^M, x_p^L) \tag{9}$$

Equation 9 is called a factorized wave model, because the unknown leak parameters (i.e., s_p^L and x_p^L), to be estimated by the measured pressure head $h(x^M)$, are separated.

Note that the factorized wave model in Equation 9 is formulated from the linear superposition-based model in Equation 6, where the hydraulic properties (i.e., q and h) at all external nodes in $V_{ex}\backslash V_s$ should be known as priors. To estimate these hydraulic properties, one pressure sensor must be placed within each external pipe of the buried tree network. However, the accessibility of all external pipes can be hardly achieved in underground pipe systems. The inaccessibility of any one external pipe would result in the complete invalidity of the MFP method for leak localization proposed by Wang et al. (2021).

Example 2. As shown in Figure 2, to formulate the factorized wave model, two additional Sensors M1 and M3 (except Sensor M2 next to the wave source) are placed near Node (1) and at Node (4), respectively. The pressure head of Node (1), that is a reservoir, and discharge of Node (4), that is a dead end, are assumed to be $h\left(x_1^U\right) = 0$ and $q\left(x_3^U\right) = 0$, respectively. The unknown discharge $q\left(x_1^U\right)$ at Node (1) and pressure head $h\left(x_3^U\right)$ at Node (4) can be computed from measured pressure heads $h\left(x_1^M\right)$ and $h\left(x_3^M\right)$ as (Kashima et al., 2013):

$$q\left(x_1^U\right) = \frac{h\left(x_1^M\right)}{F_{21}\left(x_1^U \to x_1^M\right)} \tag{10}$$

$$h\left(x_3^U\right) = h\left(x_3^M\right) \tag{11}$$

where x_p^M = local spatial coordinate of the pressure sensor in Pipe $[p]$.

There are two unique paths $R_{1,3} = \{[1], [2]\}$ and $R_{4,3} = \{[3], [2]\}$ between $N_{ex} - 1 = 2$ external nodes except the wave source, that is, $V_{ex}\backslash V_s = \{(1), (4)\}$, and the wave source, that is, $V_s = \{(3)\}$. The mass conservation at the internal Node (2) is $q\left(x_2^U\right) = q\left(x_1^D\right) + q\left(x_3^D\right)$; thus, $\alpha_1 = 0$ and $\alpha_2 = 0$. Therefore, once the q and h at $V_{ex}\backslash V_s$ are known, the q and h at the wave source V_s can be represented by $V_{ex}\backslash V_s$ as

$$\begin{aligned}\begin{bmatrix} q\left(x_2^M\right) \\ h\left(x_2^M\right) \end{bmatrix} &= \mathbf{F}\left(x_2^U \to x_2^M\right)\left\{\left(\mathbf{P}_{22} + (-1)^0\mathbf{P}_{11}\right)\mathbf{F}\left(x_1^U \to x_1^D\right)\begin{bmatrix} q\left(x_1^U\right) \\ h\left(x_1^U\right) \end{bmatrix} + (-1)^0\mathbf{P}_{11}\mathbf{F}\left(x_3^U \to x_3^D\right)\begin{bmatrix} q\left(x_3^U\right) \\ h\left(x_3^U\right) \end{bmatrix}\right\} \\ &= \underbrace{\mathbf{F}\left(x_2^U \to x_2^M\right)\mathbf{F}\left(x_1^U \to x_1^D\right)\begin{bmatrix} q\left(x_1^U\right) \\ h\left(x_1^U\right) \end{bmatrix}}_{\text{Term I}} + \underbrace{\mathbf{F}\left(x_2^U \to x_2^M\right)\mathbf{P}_{11}\mathbf{F}\left(x_3^U \to x_3^D\right)\begin{bmatrix} q\left(x_3^U\right) \\ h\left(x_3^U\right) \end{bmatrix}}_{\text{Term II}}\end{aligned} \tag{12}$$

In Equation 12, Term I represents the wave propagation from Node (1) to Node (3) without the effect of Pipe [3]; and Term II represents the wave scattering due to Pipe [3], which is caused by flow discontinuity in Path $R_{1,3}$ at Node (2).

When there is no leak in the tree network, Equation 12 becomes

$$\begin{aligned}\begin{bmatrix} q^{NL}\left(x_2^M\right) \\ h^{NL}\left(x_2^M\right) \end{bmatrix} &= \mathbf{F}^{NL}\left(x_2^U \to x_2^M\right)\mathbf{F}^{NL}\left(x_1^U \to x_1^D\right)\begin{bmatrix} q\left(x_1^U\right) \\ h\left(x_1^U\right) \end{bmatrix} \\ &\quad + \mathbf{F}^{NL}\left(x_2^U \to x_2^M\right)\mathbf{P}_{11}\mathbf{F}^{NL}\left(x_3^U \to x_3^D\right)\begin{bmatrix} q\left(x_3^U\right) \\ h\left(x_3^U\right) \end{bmatrix}\end{aligned} \tag{13}$$

When there is a leak in Pipe [1], the field matrices of Pipes [1], [2], and [3] are

$$\begin{cases}\mathbf{F}\left(x_1^U \to x_1^D\right) = \mathbf{F}^{NL}\left(x_1^U \to x_1^D\right) + s_1^L\mathbf{F}^{SL}\left(x_1^U \to x_1^L \to x_1^D\right) \\ \mathbf{F}\left(x_2^U \to x_2^D\right) = \mathbf{F}^{NL}\left(x_2^U \to x_2^D\right) \\ \mathbf{F}\left(x_3^U \to x_3^D\right) = \mathbf{F}^{NL}\left(x_3^U \to x_3^D\right)\end{cases} \tag{14}$$

Substituting Equation 14 to Equation 12 gives

$$\begin{bmatrix} q\left(x_2^M\right) \\ h\left(x_2^M\right) \end{bmatrix} = \begin{bmatrix} q^{NL}\left(x_2^M\right) \\ h^{NL}\left(x_2^M\right) \end{bmatrix} + s_1^L \mathbf{F}^{NL}\left(x_2^U \to x_2^M\right) \mathbf{F}^{SL}\left(x_1^U \to x_1^L \to x_1^D\right) \begin{bmatrix} q\left(x_1^U\right) \\ h\left(x_1^U\right) \end{bmatrix} \tag{15}$$

Equation 15 follows the form of Equation 8, whose second row gives the factorized wave model as

$$h\left(x_2^M\right) = h^{NL}\left(x_2^M\right) + s_1^L G\left(x_2^M, x_1^L\right) \tag{16}$$

Note that the concrete form of $G\left(x_2^M, x_1^L\right)$ is derived by substituting field matrix elements to Equation 15, whose detailed derivation steps are given in Appendix A. Likewise, the same form of factorized wave model in Equation 16 can be obtained when the leak is in Pipe [2] and Pipe [3].

Example 2 indicates that the factorized wave model in Equation 16 is formulated from the linear superposition-based model in Equation 12, where q and h at $V_{ex}\backslash V_s = \{(1), (4)\}$ should be known as priors. To estimate these hydraulic properties via Equations 10 and 11, as shown in Figure 2, Sensors M1 and M3 must be placed in external Pipes [1] and [3], respectively. However, the inaccessibility of Pipe [1] or Pipe [3] in an underground network would result in the complete invalidity of the factorized wave model and the MFP method for leak localization proposed by Wang et al. (2021).

2.4. Modified Factorized Transient Wave Model for Tree Networks

This sub-section formulates a modified factorized wave model for tree networks, based on which the MFP method can be implemented for leak localization without the strict accessibility requirements of all external pipes.

As shown in Figure 3, in the original model (Wang et al., 2021), the discharge of the mother pipe is the discharge summation of all its child pipes (i.e., Equation 5). This requires to place one pressure sensor in each external pipe to determine hydraulic properties q and h at each external node in $V_{ex}\backslash V_s$. To reduce the dependency upon external nodes, the wave propagation in the external pipe, which is the first child pipe of the internal Node (v^J), can be lumped into a point matrix $\mathbf{P}_b$. This allows the computation of wave propagation across the internal Node (v^J) from x^{JD} to x^{JU} without pressure measurement in this external pipe, which is termed a *non-measured external pipe*, where x^{JD} = common spatial coordinate of $I_c - 1$ child pipes except the first child pipe.

For example, in Figure 1, Pipes [2], [6], and [9]/[11] are non-measured external pipes, but Pipe [8] is not since it is the only child pipe of the internal Node (5). The number of non-measured external pipes equals the number of the internal nodes whose first child pipe is an external pipe, which is represented by N_{in}^{ex}. Therefore, the theoretical number of pressure sensors required for implementation of the MFP method in a general tree network can be reduced by N_{in}^{ex}.

The mass and momentum equations across the internal Node (v^J) connected to a non-measured external pipe become

$$\begin{bmatrix} q\left(x^{JU}\right) \\ h\left(x^{JU}\right) \end{bmatrix} = \mathbf{P}_b\left(x^{JD} \to x^{JU}\right) \left\{ \mathbf{P}_{22} \begin{bmatrix} q\left(x_2^{JD}\right) \\ h\left(x_2^{JD}\right) \end{bmatrix} + \sum_{i=2}^{I_c} (-1)^{\alpha_i} \mathbf{P}_{11} \begin{bmatrix} q\left(x_i^{JD}\right) \\ h\left(x_i^{JD}\right) \end{bmatrix} \right\} \tag{17}$$

where $\mathbf{P}_b(x^{JD} \to x^{JU})$ = point matrix of the non-measured external pipe depicting the wave propagation across the internal Node (v^J) (i.e., wave propagation from $I_c - 1$ child pipes to the mother pipe).

Thus, the q and h at the wave source can be represented by $N_{ex} - 1 - N_{in}^{ex}$ external nodes as

$$\begin{bmatrix} q\left(x^M\right) \\ h\left(x^M\right) \end{bmatrix} = \sum_{n=1}^{N_{ex}-N_{in}^{ex}-1} \mathbf{F}\left(x_{n_{l_n}}^U \to x^M\right) \left[\prod_{j=l_n-1}^{1} \mathbf{P}'^{(n_j)} \mathbf{F}\left(x_{n_j}^U \to x_{n_j}^D\right) \right] \begin{bmatrix} q\left(x_{n_1}^U\right) \\ h\left(x_{n_1}^U\right) \end{bmatrix} \tag{18}$$

where $\mathbf{P}'^{(n_j)} = \mathbf{P}_b\left[\mathbf{P}_{22} + (-1)^{\alpha_{n_j}} \mathbf{P}_{11}\right]$ if n_j is the second child pipe of the internal node connected to a non-measured external pipe, otherwise $\mathbf{P}'^{(n_j)} = \mathbf{P}_b\left[(-1)^{\alpha_{n_j}} \mathbf{P}_{11}\right]$ for other child pipes; $\mathbf{P}'^{(n_j)} = \mathbf{P}_{22} + (-1)^{\alpha_{n_j}} \mathbf{P}_{11}$ if n_j is the first child pipe of the internal node without direct connection to non-measured external pipes, otherwise $\mathbf{P}'^{(n_j)} = (-1)^{\alpha_{n_j}} \mathbf{P}_{11}$.

The concrete form of the point matrix for a non-measured external pipe depends on the specific type of boundary it connects with. If the upstream end of an intact non-measured external pipe is a dead end, its point matrix $\mathbf{P}_b$ is in the following form (detailed derivation procedures are given in Appendix B)

$$\mathbf{P}_b^{NL}\left(x^{JD} \to x^{JU}\right) = \begin{bmatrix} 1 & (-1)^{\alpha_1}\frac{F_{12}(L_p)}{F_{22}(L_p)} \\ 0 & 1 \end{bmatrix} \tag{19}$$

When there is a leak in the non-measured external pipe, its point matrix $\mathbf{P}_b$ becomes

$$\mathbf{P}_b^{WL}\left(x^{JD} \to x^{JU}\right) = \begin{bmatrix} 1 & (-1)^{\alpha_1}\frac{F_{12}(L_p)+s_p^L F_{12}^{SL}\left(x_p^L\right)}{F_{22}(L_p)+s_p^L F_{22}^{SL}\left(x_p^L\right)} \\ 0 & 1 \end{bmatrix} \tag{20}$$

The matrix component on the first row and second column of $\mathbf{P}_b^{WL}$ in Equation 20 is

$$\begin{aligned}
\left(\mathbf{P}_b^{WL}\right)_{12} &= (-1)^{\alpha_1}\frac{F_{12}(L_p) + s_p^L F_{12}^{SL}\left(x_p^L\right)}{F_{22}(L_p) + s_p^L F_{22}^{SL}\left(x_p^L\right)} \\
&= (-1)^{\alpha_1}\frac{F_{12}(L_p) + s_p^L F_{12}^{SL}\left(x_p^L\right)}{F_{22}(L_p)\left[1 + s_p^L\frac{F_{22}^{SL}\left(x_p^L\right)}{F_{22}(L_p)}\right]} \\
&= (-1)^{\alpha_1}\frac{F_{12}(L_p) + s_p^L F_{12}^{SL}\left(x_p^L\right)}{F_{22}(L_p)\left\{1 - \left(s_p^L\right)^2\left[\frac{F_{22}^{SL}\left(x_p^L\right)}{F_{22}(L_p)}\right]^2\right\}}\left[1 - s_p^L\frac{F_{22}^{SL}\left(x_p^L\right)}{F_{22}(L_p)}\right] \\
&\approx (-1)^{\alpha_1}\frac{F_{12}(L_p) + s_p^L F_{12}^{SL}\left(x_p^L\right)}{F_{22}(L_p)}\left[1 - s_p^L\frac{F_{22}^{SL}\left(x_p^L\right)}{F_{22}(L_p)}\right] \\
&= (-1)^{\alpha_1}\frac{F_{12}(L_p) - s_p^L\frac{F_{22}^{SL}\left(x_p^L\right)F_{12}(L_p)}{F_{22}(L_p)} + s_p^L F_{12}^{SL}\left(x_p^L\right) - o\left[\left(s_p^L\right)^2\right]}{F_{22}(L_p)} \\
&\approx (-1)^{\alpha_1}\frac{F_{12}(L_p)}{F_{22}(L_p)} + (-1)^{\alpha_1}s_p^L\frac{F_{12}^{SL}\left(x_p^L\right)F_{22}(L_p) - F_{22}^{SL}\left(x_p^L\right)F_{12}(L_p)}{\left[F_{22}(L_p)\right]^2}
\end{aligned} \tag{21}$$

In Equation 21, an inherent assumption for two symbols of approximate equal is that $\left(s_p^L\right)^2 \ll 1$. This assumption is called the *small leak approximation* in this paper. It implies that the size of the unknown leak is small, which is reasonable in practical leak localization since most hidden leaks are small leaks. Note that the validity of this approximation will be justified numerically in Section 4.1.

Therefore, Equation 20 can be written as

$$\begin{aligned}
\mathbf{P}_b^{WL}\left(x^{JD} \to x^{JU}\right) &= \mathbf{P}_b^{NL}\left(x^{JD} \to x^{JU}\right) + s_p^L\mathbf{P}_b^{SL}\left(x^{JD} \to x_p^L \to x^{JU}\right) \\
&= \underbrace{\begin{bmatrix} 1 & (-1)^{\alpha_1}\frac{F_{12}(L_p)}{F_{22}(L_p)} \\ 0 & 1 \end{bmatrix}}_{\text{Leak-free matrix}} + s_p^L\underbrace{\begin{bmatrix} 0 & (-1)^{\alpha_1}\frac{F_{12}^{SL}\left(x_p^L\right)F_{22}(L_p) - F_{22}^{SL}\left(x_p^L\right)F_{12}(L_p)}{\left[F_{22}(L_p)\right]^2} \\ 0 & 0 \end{bmatrix}}_{\text{Scattering matrix}}
\end{aligned} \tag{22}$$

Equation 22 indicates that the point matrix of a non-measured external pipe can be factorized into a leak-free matrix and the leak size times a leak scattering matrix dependent on the leak location. Note that Equation 22 has the same form as Equation 3.

If there is no leak in the network, Equation 18 becomes

$$\begin{bmatrix} q^{NL}(x^M) \\ h^{NL}(x^M) \end{bmatrix} = \sum_{n=1}^{N_{ex}-N_{in}^{ex}-1} \mathbf{F}^{NL}\left(x_{n_{l_n}}^U \rightarrow x^M\right) \left[\prod_{j=l_n-1}^{1} \mathbf{P}'^{(n_j)} \mathbf{F}^{NL}\left(x_{n_j}^U \rightarrow x_{n_j}^D\right)\right] \begin{bmatrix} q(x_{n_1}^U) \\ h(x_{n_1}^U) \end{bmatrix} \tag{23}$$

When there is a leak in Pipe $[p^L]$, its transfer matrix is in the form of Equation 3 or Equation 22. Substituting it to Equation 18 results in the form of Equation 8

$$\begin{bmatrix} q(x^M) \\ h(x^M) \end{bmatrix} = \begin{bmatrix} q^{NL}(x^M) \\ h^{NL}(x^M) \end{bmatrix} + s_p^L \begin{bmatrix} q^*(x^M, x_p^L) \\ G(x^M, x_p^L) \end{bmatrix}$$

Whose second row is in the form of the factorized wave model in Equation 9

$$h(x^M) = h^{NL}(x^M) + s_p^L G(x^M, x_p^L)$$

Although the modified factorized wave model has the same form as the original one, it can still be formulated and the MFP method can be implemented if some of (or even all of) N_{in}^{ex} external pipes are inaccessible.

Example 3. As shown in Figure 2, Pipe [1] or Pipe [3] can be defined as the first child pipe of the internal Node (2), depending on their inaccessibility, which is the non-measured external pipe. If Pipe [3] is inaccessible and is the non-measured external pipe, whose upstream end x_3^U is bounded by a dead end, the hydraulic properties before (i.e., x_1^D) and after (i.e., x_2^U) the internal Node (2) are linked as

$$\begin{bmatrix} q(x_2^U) \\ h(x_2^U) \end{bmatrix} = \mathbf{P}_b(x_1^D \rightarrow x_2^U) \begin{bmatrix} q(x_1^D) \\ h(x_1^D) \end{bmatrix} \tag{24}$$

where $\mathbf{P}_b(x_1^D \rightarrow x_2^U)$ = point matrix of Pipe [3] depicting the wave propagation crossing the internal Node (2) from x_1^D to x_2^U.

As a result, the hydraulic properties at the pressure sensor in Pipe [2] (i.e., at x_2^M) can be expressed as

$$\begin{bmatrix} q(x_2^M) \\ h(x_2^M) \end{bmatrix} = \mathbf{F}(x_2^U \rightarrow x_2^M)\, \mathbf{P}_b(x_1^D \rightarrow x_2^U)\, \mathbf{F}(x_1^U \rightarrow x_1^D) \begin{bmatrix} q(x_1^U) \\ h(x_1^U) \end{bmatrix} \tag{25}$$

Equation 25 indicates that if Pipe [3] is inaccessible, which means the hydraulic properties at the external Node (4) (i.e., x_3^U) cannot be measured by or computed from a placed pressure sensor in it, the hydraulic properties at x_2^M can be represented solely by the external Node (1) (i.e., x_1^U).

When there is no leak in the pipe network, Equation 25 becomes

$$\begin{bmatrix} q^{NL}(x_2^M) \\ h^{NL}(x_2^M) \end{bmatrix} = \mathbf{F}^{NL}(x_2^U \rightarrow x_2^M)\, \mathbf{P}_b^{NL}(x_1^D \rightarrow x_2^U)\, \mathbf{F}^{NL}(x_1^U \rightarrow x_1^D) \begin{bmatrix} q(x_1^U) \\ h(x_1^U) \end{bmatrix} \tag{26}$$

For Pipe $[p^L]$ with a leak, its transfer matrix is in the form of Equation 3 or Equation 22. This means that $\left[q(x_2^M), h(x_2^M)\right]^\top$ in Equation 25 can be decomposed into a term independent of leak parameters and a term dependent on leak parameters. For instance,

Condition I. Leak in Pipe [1]
When the leak is in Pipe [1], the field matrix of Pipe [1] is

$$\mathbf{F}(x_1^U \rightarrow x_1^D) = \mathbf{F}^{WL}(x_1^U \rightarrow x_1^D) = \mathbf{F}^{NL}(x_1^U \rightarrow x_1^D) + s_1^L \mathbf{F}^{SL}(x_1^U \rightarrow x_1^L \rightarrow x_1^D) \tag{27}$$

Substituting Equation 27 to Equation 25 results in

$$\begin{bmatrix} q\left(x_2^M\right) \\ h\left(x_2^M\right) \end{bmatrix} = \begin{bmatrix} q^{NL}\left(x_2^M\right) \\ h^{NL}\left(x_2^M\right) \end{bmatrix} + s_1^L \mathbf{F}^{NL}\left(x_2^U \to x_2^M\right) \mathbf{P}_b^{NL}\left(x_1^D \to x_2^U\right) \mathbf{F}^{SL}\left(x_1^U \to x_1^L \to x_1^D\right) \begin{bmatrix} q\left(x_1^U\right) \\ h\left(x_1^U\right) \end{bmatrix} \tag{28}$$

Condition II. Leak in Pipe [2]

When the leak is in Pipe [2], the field matrix of Pipe [2] is

$$\mathbf{F}\left(x_2^U \to x_2^M\right) = \mathbf{F}^{WL}\left(x_2^U \to x_2^M\right) = \mathbf{F}^{NL}\left(x_2^U \to x_2^M\right) + s_2^L \mathbf{F}^{SL}\left(x_2^U \to x_2^L \to x_2^M\right) \tag{29}$$

Substituting Equation 29 into Equation 25 results in

$$\begin{bmatrix} q\left(x_2^M\right) \\ h\left(x_2^M\right) \end{bmatrix} = \begin{bmatrix} q^{NL}\left(x_2^M\right) \\ h^{NL}\left(x_2^M\right) \end{bmatrix} + s_2^L \mathbf{F}^{SL}\left(x_2^U \to x_2^L \to x_2^M\right) \mathbf{P}_b^{NL}\left(x_1^D \to x_2^U\right) \mathbf{F}^{NL}\left(x_1^U \to x_1^D\right) \begin{bmatrix} q\left(x_1^U\right) \\ h\left(x_1^U\right) \end{bmatrix} \tag{30}$$

Condition III. Leak in Pipe [3]

When the leak is in Pipe [3], the point matrix crossing the internal Node (2) can be expressed as

$$\mathbf{P}_b^{WL}\left(x_1^D \to x_2^U\right) = \mathbf{P}_b^{NL}\left(x_1^D \to x_2^U\right) + s_3^L \mathbf{P}_b^{SL}\left(x_1^D \to x_3^L \to x_2^U\right) \tag{31}$$

Substituting Equation 31 to Equation 25 results in

$$\begin{bmatrix} q\left(x_2^M\right) \\ h\left(x_2^M\right) \end{bmatrix} = \begin{bmatrix} q^{NL}\left(x_2^M\right) \\ h^{NL}\left(x_2^M\right) \end{bmatrix} + s_3^L \mathbf{F}^{NL}\left(x_2^U \to x_2^M\right) \mathbf{P}_b^{SL}\left(x_1^D \to x_3^L \to x_2^U\right) \mathbf{F}^{NL}\left(x_1^U \to x_1^D\right) \begin{bmatrix} q\left(x_1^U\right) \\ h\left(x_1^U\right) \end{bmatrix} \tag{32}$$

The second rows of Equations 28, 30, and 32 can be expressed as

$$h\left(x_2^M\right) = h^{NL}\left(x_2^M\right) + s_p^L G\left(x_2^M, x_p^L\right) \tag{33}$$

Example 3 indicates that the modified factorized wave model can still be formulated, even if the external Pipe [3] (or Pipe [1]) in Figure 2 is inaccessible.

3. Leak Localization Algorithm

Based on the modified factorized wave model, this section proposes an efficient and robust MFP algorithm to localize the unknown leak in tree networks using the measured pressure signals. Note that waves at all frequencies do not carry equally effective information for leak localization; thus, this section will first identify unwanted frequencies and then minimize information at these frequencies, where the measurement noise is amplified.

Let h_j^M be the measured pressure head $h(x^M)$ at frequency ω_j, which is contaminated by a noise n_j as

$$h_j^M = h^{NL}\left(x^M, \omega_j\right) + s_p^L G\left(x^M, x_p^L, \omega_j\right) + n_j \tag{34}$$

Table 1
System Parameters of the Tree Network in Figure 2

Parameter	L_1(m)	L_2(m)	L_3(m)	D_1(m)	D_2(m)	D_3(m)	a(m/s)	f_{DW}	Q_0(m^3/s)
Value	200	300	400	0.25	0.25	0.25	1,000	0.02	0.02

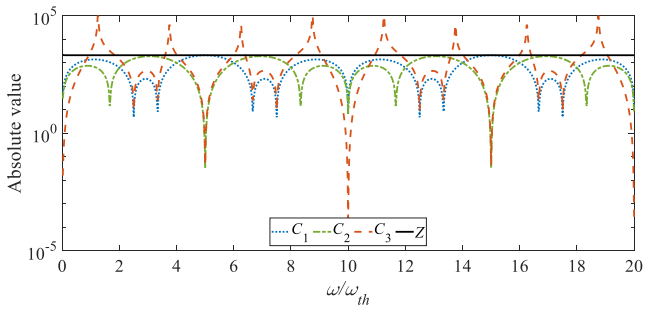

Figure 4. Amplification coefficients of measurement noise (C_1, C_2, and C_3) and pipe impedance (Z).

Equation 34 can be further expressed as

$$\Delta h_j = h_j^M - h^{NL}\left(x^M, \omega_j\right) = s_p^L G\left(x^M, x_p^L, \omega_j\right) + n_j \tag{35}$$

where Δh_j = leak-induced pressure difference at frequency ω_j.

The leak-induced pressure difference $\Delta\mathbf{h}$ at all J frequencies is

$$\Delta\mathbf{h} = \mathbf{h}^M - \mathbf{h}^{NL}\left(x^M\right) = s_p^L \mathbf{G}\left(x^M, x_p^L\right) + \mathbf{n} \tag{36}$$

where $\mathbf{h}^M = \left(h_1^M, \ldots, h_J^M\right)^\top$; $\mathbf{h}^{NL}\left(x^M\right) = \left[h^{NL}\left(x^M, \omega_1\right), \ldots, h^{NL}\left(x^M, \omega_J\right)\right]^\top$ is computed from the transient model in Equation 23; $\mathbf{G}\left(x^M, x_p^L\right) = \left[G\left(x^M, x_p^L, \omega_1\right), \ldots, G\left(x^M, x_p^L, \omega_J\right)\right]^\top$; $\mathbf{n} = (n_1, \ldots, n_J)^\top$ is random noise vector assumed to follow the zero-mean Gaussian distribution $\mathcal{N}\left(\mathbf{0}, \sigma^2 \mathbf{I}_J\right)$, where $\mathbf{I}_J = J$-dimensional identity matrix. Note that the target signal $\Delta\mathbf{h}$ can be computed by the first equal sign of Equation 36 based on the known pressure measurements, and the second equal sign represents the theoretical model of $\Delta\mathbf{h}$ with leak parameters s_p^L and x_p^L.

3.1. Identification and Minimization of Amplified Measurement Noise

This sub-section identifies and minimizes the unwanted frequencies, at which the measurement noise is amplified in the target signal $\Delta\mathbf{h}$.

As shown in Equation 23, at frequency ω_j, the $h^{NL}(x^M)$ in Equation 35 is computed from hydraulic properties at external nodes, which have been contaminated by measurement noise of pressure sensors. Therefore, there is also noise in $h^{NL}(x^M)$.

Example 4. For the tree network in Figure 2, the $h^{NL}\left(x_2^M\right)$ in Equation 26 is computed from hydraulic properties at the external Node (1), that is, $q\left(x_1^U\right)$ and $h\left(x_1^U\right)$, which have been contaminated by measurement noise of Sensor M1 as (detailed derivation procedures are in Appendix C)

$$\begin{aligned}\tilde{h}^{NL}\left(x_2^M, \omega_j\right) = h^{NL}\left(x_2^M, \omega_j\right) &+ \underbrace{F_{21}(L_2, \omega_j)\, F_{11}(L_1, \omega_j)}_{C_1(\omega_j)} \delta q(\omega_j) \\ &+ \underbrace{F_{22}(L_2, \omega_j)\, F_{21}(L_1, \omega_j)}_{C_2(\omega_j)} \delta q(\omega_j) \\ &+ \underbrace{F_{21}(L_2, \omega_j)\, F_{21}(L_1, \omega_j)\, \frac{F_{12}(L_3, \omega_j)}{F_{22}(L_3, \omega_j)}}_{C_3(\omega_j)} \delta q(\omega_j)\end{aligned} \tag{37}$$

where $\tilde{h}^{NL}$ is h^{NL} with noise; δq = measurement noise into $q\left(x_1^U\right)$; and C_1, C_2, and C_3 = amplification coefficients of measurement noise.

For a specific tree network with known parameters in Table 1, the amplification coefficients (C_1, C_2, and C_3) and the pipe impedance Z are plotted in Figure 4. The frequency ω in the x-axis is normalized by the theoretical frequency of the tree network $\omega_{th} = 2\pi a/[4(L_1 + L_2)]$. Note that the impedance Z physically transforms q to h without any amplification. It is evident that both C_1 and C_2 are well bounded by the pipe impedance Z, whereas C_3 is much larger than Z at some frequencies, where the measurement noise δq is significantly amplified. The amplified noise in $\tilde{h}^{NL}$ changes the overall shape of the target signal $\Delta\mathbf{h}$, resulting in the inaccuracy or even invalidity of the modified factorized wave model. Therefore, the unwanted frequencies ω_j where measurement noise is amplified should be identified and filtered by

$$Z(\omega_j) \le \max\left[C_1(\omega_j), C_2(\omega_j), C_3(\omega_j)\right] \tag{38}$$

Note that although the modified factorized wave model can still be formulated by reducing as much as N_{in}^{ex} pressure sensors, the amount of useful information (i.e., frequencies) for leak localization is also decreased compared

with the original model in Wang et al. (2021). Therefore, the selection of the model depends on both the availability of sensors and the accessibility of external pipes. If (i) all external pipes are accessible but sensors are insufficient, or (ii) sensors are sufficient but there are inaccessible external pipes, or (iii) both sensors are insufficient and there are inaccessible external pipes, the modified model should be used; otherwise, the original model would be recommended.

3.2. Leak Localization by MFP

This sub-section localizes the unknown leak in a tree network by the MFP method based on: (i) the modified factorized wave model in Section 2; and (ii) the filtered signal in Section 3.1.

The information at unwanted frequencies are identified and filtered by Equation 38; thus, the leak-induced pressure difference $\Delta\mathbf{h}$ becomes

$$\Delta\mathbf{h}_f = s_p^L \mathbf{G}_f\left(x^M, x_p^L\right) + \mathbf{n}_f \tag{39}$$

where the subscript "f" means filtered signals without unwanted frequencies.

The optimal leak location $\hat{x^L}$ and size $\hat{s^L}$ can be estimated by the MFP method as (detailed derivation procedures are given in Appendix D)

$$\hat{x_p^L} = \arg\max_{x_p^L} |B|^2 = \arg\max_{x_p^L} \frac{\Delta\mathbf{h}_f^{\mathrm{H}} \mathbf{G}_f\left(x_p^L\right) \mathbf{G}_f^{\mathrm{H}}\left(x_p^L\right) \Delta\mathbf{h}_f}{\mathbf{G}_f^{\mathrm{H}}\left(x_p^L\right) \mathbf{G}_f\left(x_p^L\right)} \tag{40}$$

$$\hat{s_p^L} = \frac{\mathbf{G}_f^{\mathrm{H}}\left(\hat{x_p^L}\right) \Delta\mathbf{h}_f}{\mathbf{G}_f^{\mathrm{H}}\left(\hat{x_p^L}\right) \mathbf{G}_f\left(\hat{x_p^L}\right)} \tag{41}$$

where $|B|^2$ = objective function; "arg max" = the arguments of the maxima; and the superscript "H" = conjugate transpose.

The leak is localized by plotting the objective function $|B|^2$ along each pipe of the tree network, which is an one-dimensional (1D) search of the optimal leak location $\hat{x_p^L}$. The computation of the proposed leak localization algorithm is highly efficient, because (i) a 2D optimization problem is reduced into two 1D search problems, where the leak location and size are estimated separately and sequentially; and (ii) the frequency domain wave model is essentially an analytical model.

The detailed implementation procedures of the MFP method for leak localization in a general tree network based on the modified factorized wave model is summarized in Algorithm 1.

Algorithm 1. Leak Localization in a Tree Network Based on the Modified Factorized Wave Model

1. Check the accessibility of external pipes and availability of pressure sensors and determine the sensor placement strategy.
2. Calculate $q\left(x_{n_1}^U\right)$ and $h\left(x_{n_1}^U\right)$ for all external pipes other than non-measured external pipes (e.g., via Equations 10 and 11).
3. Compute $h^{NL}(x^M)$ by Equation 23 for J frequencies and pressure head difference $\Delta\mathbf{h}$ by Equation 36.
4. Derive noise amplification coefficients and filter out unwanted frequencies, giving $\Delta\mathbf{h}_f$, $\mathbf{G}_f$, and $\mathbf{n}_f$ (e.g., via Equation 38).
5. Plot the objective function $|B|^2$ in Equation 40 with respect to x_p^L along all pipes of the tree network, where the x_p^L has the maximum $|B|^2$ is the estimated leak location.
6. Estimate the leak size by Equation 41.

Table 2
Parameters of Numerical Tests: Justification of the Small Leak Approximation

Test	p^L	x_p^L (m)	s_p^L(m^2)	Q_0^L(m^3/s)	Q_0^L/Q_0
J1	3	200	2×10^{-5}	5×10^{-4}	2.5%
J2	3	200	2×10^{-4}	5×10^{-3}	25%
J3	3	200	4×10^{-4}	1×10^{-2}	50%
J4	3	320	2×10^{-5}	5×10^{-4}	2.5%
J5	3	320	2×10^{-4}	5×10^{-3}	25%
J6	3	320	4×10^{-4}	1×10^{-2}	50%

4. Numerical Tests

In this section, the validity of the small leak approximation in Section 2.4 is first justified numerically. Afterward, the proposed MFP method for leak localization based on the modified factorized wave model is preliminarily demonstrated by numerical tests conducted in noisy environments.

The simple tree network in Figure 2 is revisited in Sections 4.1–4.3 and its detailed system parameters are listed in Table 1. The lengths of three pipes are $L_1 = 200$ m, $L_2 = 300$ m, and $L_3 = 400$ m, respectively; and they all have the same pipe diameter $D_1 = D_2 = D_3 = 0.25$ m. Note that Pipe [3] is assumed to be inaccessible. The pressure wave speed in these elastic pipes is 1,000 m/s. The Darcy–Weisbach friction factor f_{DW} is 0.02. The pressure head of the upstream reservoir at x_1^U remains constant at 30 m, which implies $h(x_1^U) = 0$. The steady-state discharge from the reservoir to the tree network is 0.02 m^3/s. The pressure wave is generated by a sudden and complete closure of the downstream valve at x_2^D.

4.1. Justification of Small Leak Approximation

This sub-section numerically justifies the validity of the key small leak approximation in Section 2.4, based on which the modified factorized wave model is formulated.

To justify the approximation, as shown in Table 2, six numerical tests (i.e., Tests J1 to J6) with a leak in the non-measured external Pipe [3] are conducted. The leak is placed at two different representative locations, that is, $x_3^L = 200$ m or 320 m. Three leak sizes $s_3^L = 2\times10^{-5}$ m^2, 2×10^{-4} m^2, and 4×10^{-4} m^2 are considered, which

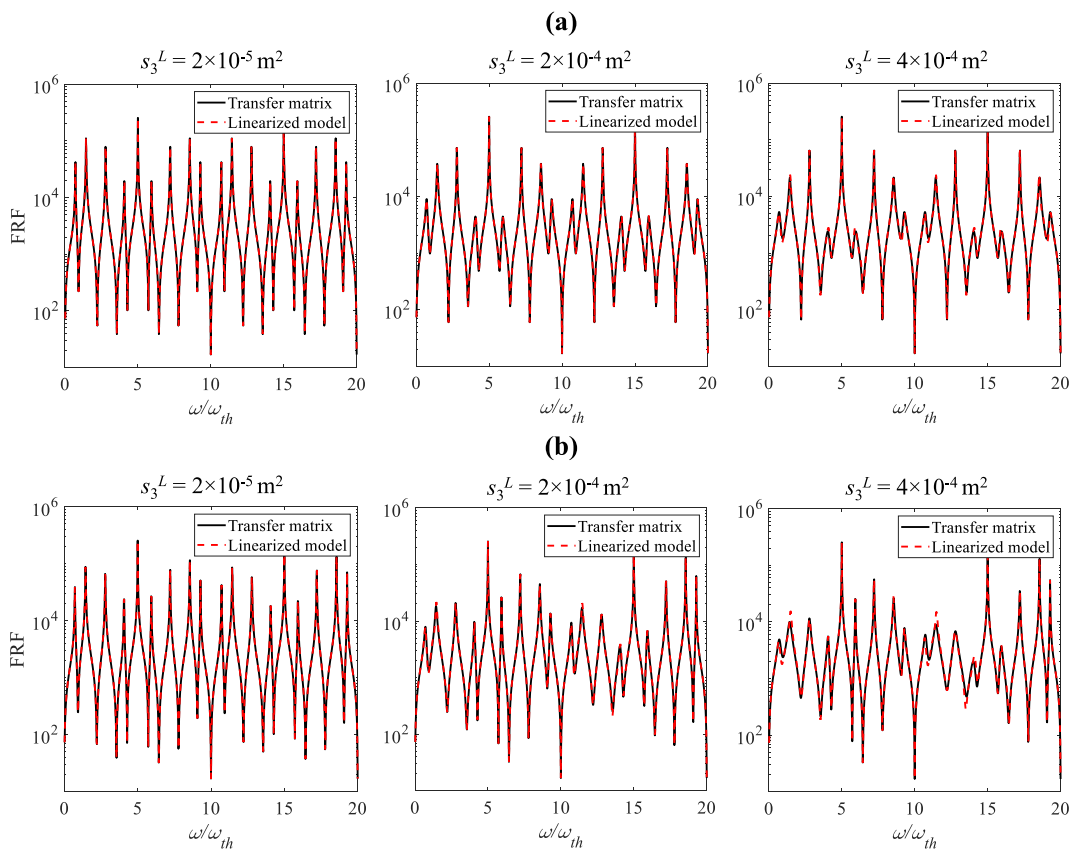

Figure 5. Frequency response functions computed by the transfer matrix and the linearized model with small leak approximation for different leak locations: (a) $x_3^L = 200$ m; and (b) $x_3^L = 320$ m.

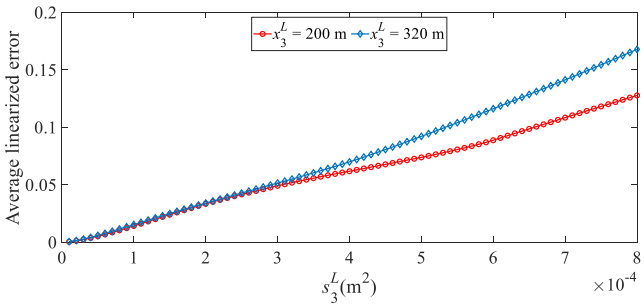

Figure 6. Average linearized error due to small leak approximation with respect to the leak size.

induces $Q_0^L/Q_0 = 2.5\%$, 25%, and 50% leakage of the total supplied water, respectively (computed by the orifice equation); where Q_0^L = steady state discharge from the leak. The FRFs at the downstream valve of all six tests are plotted in Figure 5. The solid line and dash line are computed by the transfer matrix and the linearized model with small leak approximation, respectively. For a reasonable leak size (i.e., $s_3^L = 2 \times 10^{-5}$ m^2 and 2×10^{-4} m^2), the FRFs from two models are almost indistinguishable. Even for an extremely big leak (i.e., $s_3^L = 4 \times 10^{-4}$ m^2), which leaks half of the supplied water $Q_0^L/Q_0 = 50\%$, the overall FRFs from two models are well matched except that the linearized error is relatively large at few resonant peaks.

Furthermore, the average linearized errors caused by the small leak approximation for more leak sizes are computed by Equation 42 and plotted in Figure 6.

$$\bar{\epsilon} = \frac{1}{J}\sum_{j=1}^{J} \frac{||h^{\delta}(x_2^M, \omega_j)| - |h(x_2^M, \omega_j)||}{|h(x_2^M, \omega_j)|} \tag{42}$$

where h^{δ} = computed pressure head with linearized error.

It indicates that the small leak approximation is acceptable for a leak with reasonable size: the average linearized error is less than 4% for leaks smaller than 2×10^{-4} m^2, which is equivalent to a $Q_0^L/Q_0 = 25\%$ loss of supply water from the leak.

4.2. Localization of a Single Leak

In this sub-section, the proposed MFP algorithm based on the modified factorized wave model is used to localize single leaks within a tree network in noisy environments.

As shown in Table 3, six numerical tests (i.e., Tests S1 to S6) with different leak sizes s_p^L and locations x_p^L are conducted for leaks with reasonable sizes. The measured pressure signals by Sensors M1 (i.e., at x_1^M) and Sensor M2 (i.e., at x_2^M) are used for leak localization. For example, the FRFs of two measured signals at x_1^M and x_2^M of Test S6 are plotted in Figure 7. Note that the SNR, which has been defined by Wang and Ghidaoui (2018b) in water pipes, of all the numerical tests in this section is 10 dB.

Based on FRFs at x_1^M and x_2^M, the MFP algorithm is implemented for leak localization by plotting the objective functions $|B|^2$ of Equation 40 for three pipes in Figure 8. The x-axis is the sequential connection of spatial coordinates of all three pipes. The vertical dashed lines represent the actual leak locations. It can be observed that the objective function $|B|^2$ has a globally maximum value near the actual leak location. The estimated leak locations in Tests S1 to S6 are $x_1^L = 40$ m, $x_2^L = 120$ m, $x_3^L = 240.5$ m, $x_1^L = 60$ m, $x_2^L = 150$ m, and $x_3^L = 279.5$ m, respectively; which means a leak in any pipe of the tree network can be localized accurately even though Pipe [3] is inaccessible.

Table 3
Parameters of Numerical Tests: Tree Network With a Single Leak

Test	p^L	x_p^L (m)	s_p^L(m^2)	Q_0^L(m^3/s)	Q_0^L/Q_0
S1	1	40	2×10^{-5}	5×10^{-4}	2.5%
S2	2	120	2×10^{-5}	5×10^{-4}	2.5%
S3	3	240	2×10^{-5}	5×10^{-4}	2.5%
S4	1	60	2×10^{-4}	5×10^{-3}	25%
S5	2	150	2×10^{-4}	5×10^{-3}	25%
S6	3	280	2×10^{-4}	5×10^{-3}	25%

4.3. Localization of Multiple Leaks

In this sub-section, the proposed MFP algorithm based on the modified factorized wave model is used to localize multiple co-existing leaks within a tree network in noisy environments.

Note that only a single leak is assumed in the factorized wave model, that is, Equation 39. However, it is possible to detect multiple leaks based on the single-leak model due to the fact that the objective function $|B|^2$ is a linear superposition of effects from multiple leaks, such that the 1D search can identify the multiple local optima separately. More detailed proof and explanation regarding this issue was given by Wang and Ghidaoui (2018b) with a single-pipe example.

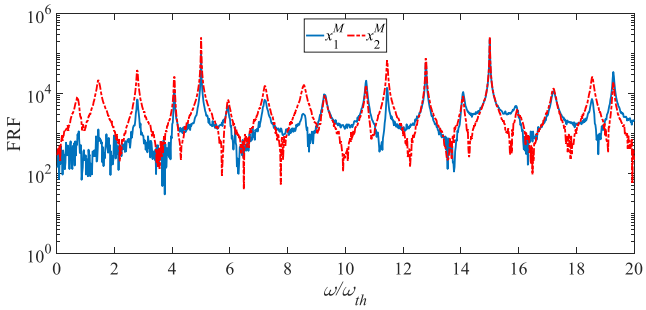

Figure 7. Frequency response functions of the measured signals at x_1^M and x_2^M.

As shown in Table 4, six numerical tests (i.e., Tests T1 to T6) for a tree network with two co-existing leaks at locations $x_p^{L_1}$ and $x_p^{L_2}$ are conducted. The measured pressure signals by Sensors M1 (i.e., at x_1^M) and Sensor M2 (i.e., at x_2^M) are used for leak localization. Based on FRFs at x_1^M and x_2^M, the proposed MFP algorithm is implemented for leak localization by plotting the objective functions $|B|^2$ of Equation 40 for three pipes in Figure 9.

In Test T1, two co-existing leaks are in Pipe [1] (i.e., $p^{L_1} = p^{L_2} = 1$) and the distance between them is 60 m, which is larger than the theoretical spatial resolution, being half the probing minimum wavelength $\lambda_{\min}/2 = (2\pi a/20\omega_{th})/2 = 50$ m. As shown in Figure 9a, two leaks can be resolved accurately. However, in Test T2, where the distance between two leaks in Pipe [1] is 20 m, which is smaller than $\lambda_{\min}/2 = 50$ m, the objective function $|B|^2$ only gives one maximum peak between two actual leak locations in Figure 9b. This is due to the diffraction limit that restricts the MFP algorithm to distinguish two anomalies separated by a distance less than half the minimum probing wavelength $\lambda_{\min}/2 = 50$ m (Wang & Ghidaoui, 2018b; Wang et al., 2021).

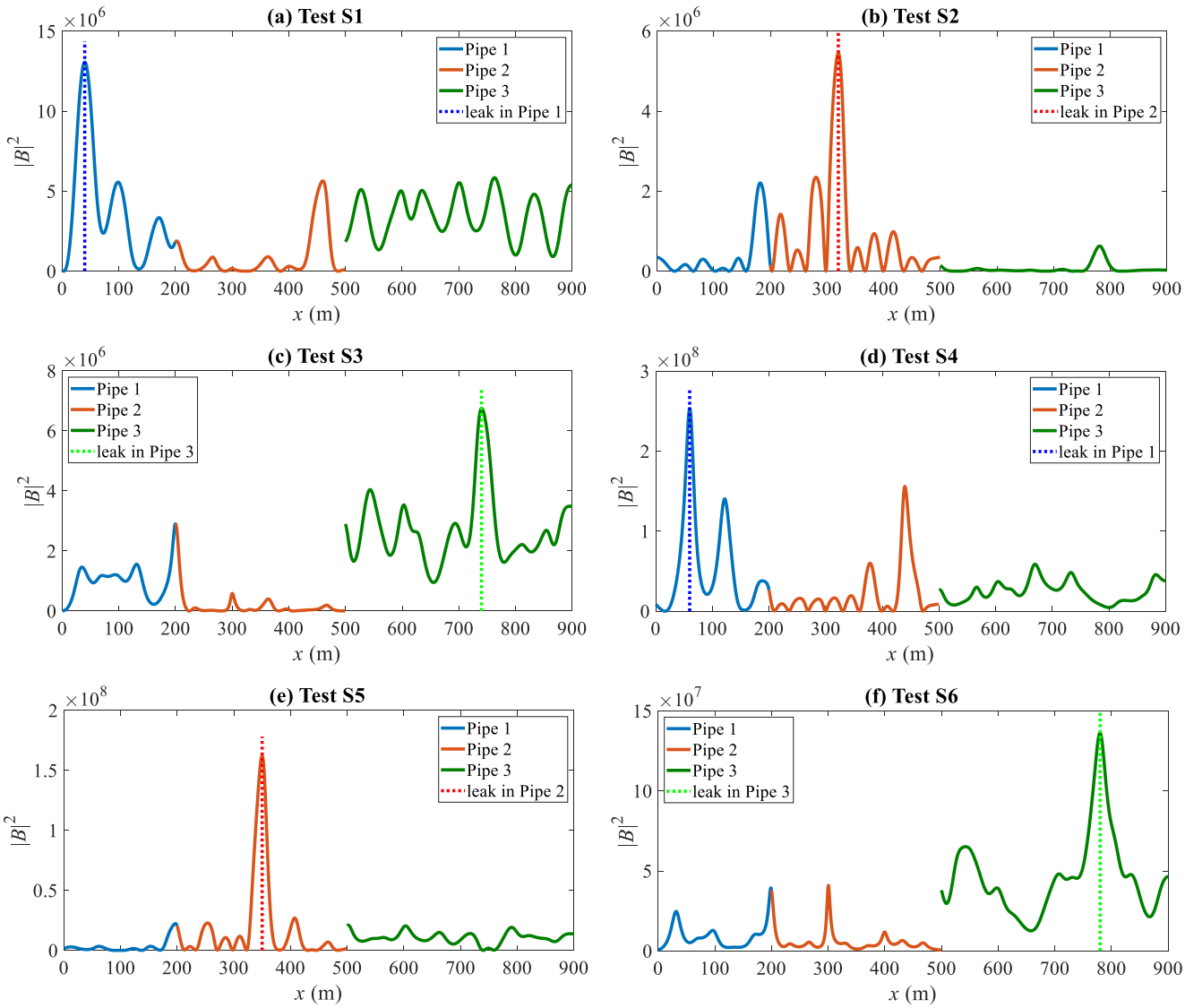

Figure 8. Localization results of single leaks: objective function of (a) Test S1; (b) Test S2; (c) Test S3, (d) Test S4, (e) Test S5, and (f) Test S6.

Table 4
Parameters of Numerical Tests: Tree Network With Two Leaks

Test	p^{L_1}	$x_p^{L_1}$ (m)	p^{L_2}	$x_p^{L_2}$ (m)
T1	1	60	1	120
T2	1	60	1	80
T3	2	90	2	210
T4	3	160	3	320
T5	1	100	3	200
T6	2	150	3	280

Figures 9c–9e indicates that two leaks in the same pipe or different pipes can be identified accurately by two global dominant peaks of the objective function $|B|^2$ even though Pipe [3] is inaccessible. However, in Figure 9f, the second dominant peak occurs in Pipe [1], which is even higher than that of the actual leak in Pipe [2]. This is because the multiple-leak localization is based on the single-leak model. Note that in a tree network with multiple leaks, the objective function with a single-leak model cannot accurately and uniquely identify all the leaks, but can guarantee a local dominant peak of the objective function near each actual leak location, which also gives a good initial guess of real leak locations. To fully determine the number and locations of multiple leaks, as done in a single pipe system by Wang and Ghidaoui (2018a), a more sophisticated model with multiple assumed leaks and corresponding leak number estimation algorithms are required. This is out of the main scope of the present paper.

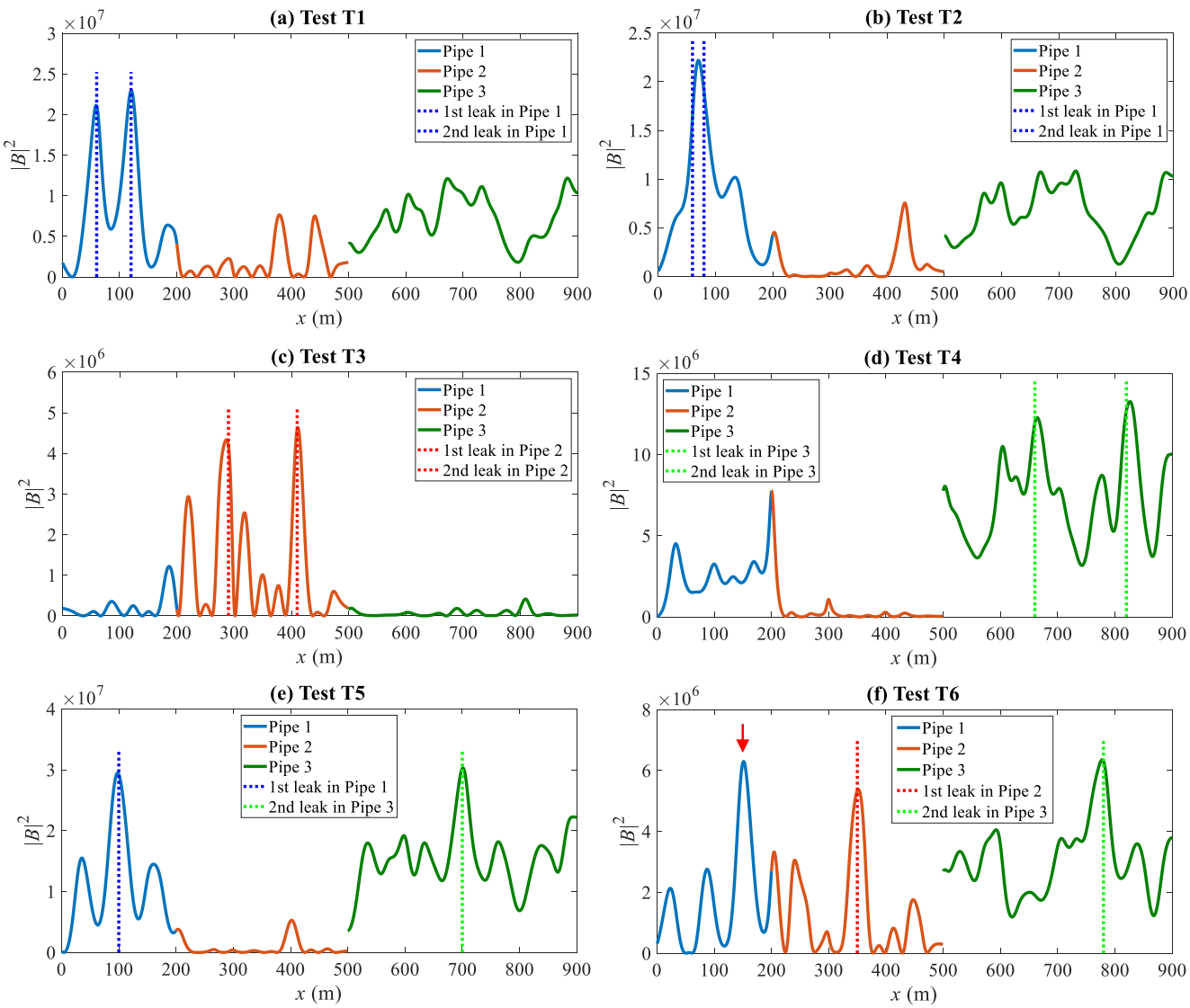

Figure 9. Localization results of two co-existing leaks: objective function for (a) Test T1, (b) Test T2, (c) Test T3, (d) Test T4, (e) Test T5, and (f) Test T6.

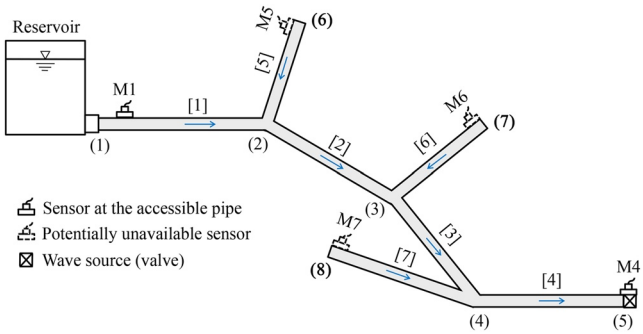

Figure 10. Graph of a relatively complex tree network with seven pipes.

4.4. Leak Localization With Different Numbers of Accessible Boundaries

In this sub-section, the proposed MFP algorithm is further extended to a more complex tree network to investigate the influence of different numbers of accessible boundaries on the leak localization accuracy in noisy environments.

As shown in Figure 10, a tree network with seven pipes and eight nodes is used for the numerical tests, whose detailed system parameters are listed in Table 5. Specifically, the diameter and the total length of the main pipe, including Pipes [1–4], are 0.25 and 1,000 m, respectively. The lengths of 3 branch pipes, namely Pipes [5–7], are 150, 100, and 150 m, respectively. A leak with the size $s_3^L = 2 \times 10^{-5}$ m^2 is located at 45 m away from Node (3) in Pipe [3] (i.e., $x_3^L = 45$ m). As shown in Table 6, six tests (i.e., Tests N1 to N4′) with different numbers of accessible branch pipes or available sensors are conducted. For example, in Test N3, Pipes [5] and [6] are assumed to be inaccessible; thus, the pressure signals can only be measured by available Sensors M1, M4, and M7. Based on FRFs at available sensors in Table 6, the proposed MFP algorithm is implemented for leak localization by plotting the objective functions $|B|^2$ along seven pipes in Figure 11.

In Test N1, all boundaries are accessible; thus, there is no amplified noise in $\tilde{h}^{NL}\left(x_4^M, \omega_j\right)$ at each frequency ω_j. Figure 11a is computed utilizing the measured signals at all frequencies, which accurately localize the unknown leak. In Test N2, when Pipe [5] is assumed to be inaccessible, as discussed in Section 3.1, amplified noise starts to occur at certain frequencies. Figure 11b is also computed utilizing the measured signals at all frequencies. Fortunately, the leak location can still be estimated accurately, since the noise at only a small portion of frequencies is amplified. However, as the number of inaccessible boundaries increases in Tests N3 and N4, waves at more frequencies are contaminated by amplified noise. If wave information at all frequencies is used, the leak localization method would become totally invalid. For example, Figures 11c and 11d indicate that the leak locations in Tests N3 and N4 are wrongly estimated in Pipes [6] and [5], respectively. To address this problem, in Tests N3′ and N4′, the unwanted frequencies with amplified noise of Tests N3 and N4 are identified and discarded by Step 4 of Algorithm 1. The objective functions without unwanted frequencies are plotted in Figures 11e and 11f, where the leak can still be pinpointed by the proposed Algorithm 1. Note that although the proposed MFP algorithm also gives the right leak location with less boundary measurements, Tests N3′ and N4′ produce relatively higher side lobes than Test N1, which is equipped with five sensors.

5. Experimental Tests

In this section, the proposed MFP algorithm for leak localization based on the modified factorized wave model is verified by experimental tests conducted in the Water Resources Research Laboratory of the Hong Kong University of Science and Technology (HKUST). Note that the experimental data are almost the same with Wang et al. (2021), except that only two among all three sensors are used due to the assumed inaccessibility of Pipe [3].

The overall layout and simplified sketch of the tree network are shown in Figure 12. The upstream end of Pipe [1] (i.e., at x_1^U) and downstream end of Pipe [2] (i.e., at x_2^D) are bounded by a centrifugal pump and valve, respectively. The upstream end of Pipe [3] (i.e., at x_3^U) is a dead end. The lengths of Pipes [1], [2], and [3] are $L_1 = 13.88$, $L_2 = 128$, and $L_3 = 25$ m, respectively. All pipes have the same diameter $D_1 = D_2 = D_3 = 0.0792$ m. The pipe wall is made from high-density polyethylene (HDPE) material, whose detailed viscoelastic parameters (Covas et al., 2005) are summarized in Table 7. The leak is placed in Pipe [2], which is 30 m away from the internal Node (2). The steady-state discharge before and after the leak are 1.5×10^{-3} m^3/s and 1.0×10^{-3} m^3/s, respectively.

Table 5
System Parameters of the Tree Network in Figure 10

Parameter	L_1 (m)	L_2 (m)	L_3 (m)	L_4 (m)	L_5 (m)	L_6 (m)	L_7 (m)	D_1–D_4 (m)	D_5–D_7 (m)	a (m/s)	f_{DW}	Q_0 (m^3/s)
Value	300	200	150	350	150	100	150	0.25	0.20	1,000	0.02	0.02

Table 6
Parameters of Numerical Tests: Tree Network With Different Numbers of Accessible Boundaries

Test	Inaccessible Pipe	Available Sensor	Utilized Wave Information
N1	No	M1, M4, M5, M6, and M7	Information at all frequencies
N2	[5]	M1, M4, M6, and M7	Information at all frequencies
N3	[5] and [6]	M1, M4, and M7	Information at all frequencies
N3′	[5] and [6]	M1, M4, and M7	Discarding unwanted frequencies
N4	[5], [6], and [7]	M1 and M4	Information at all frequencies
N4′	[5], [6], and [7]	M1 and M4	Discarding unwanted frequencies

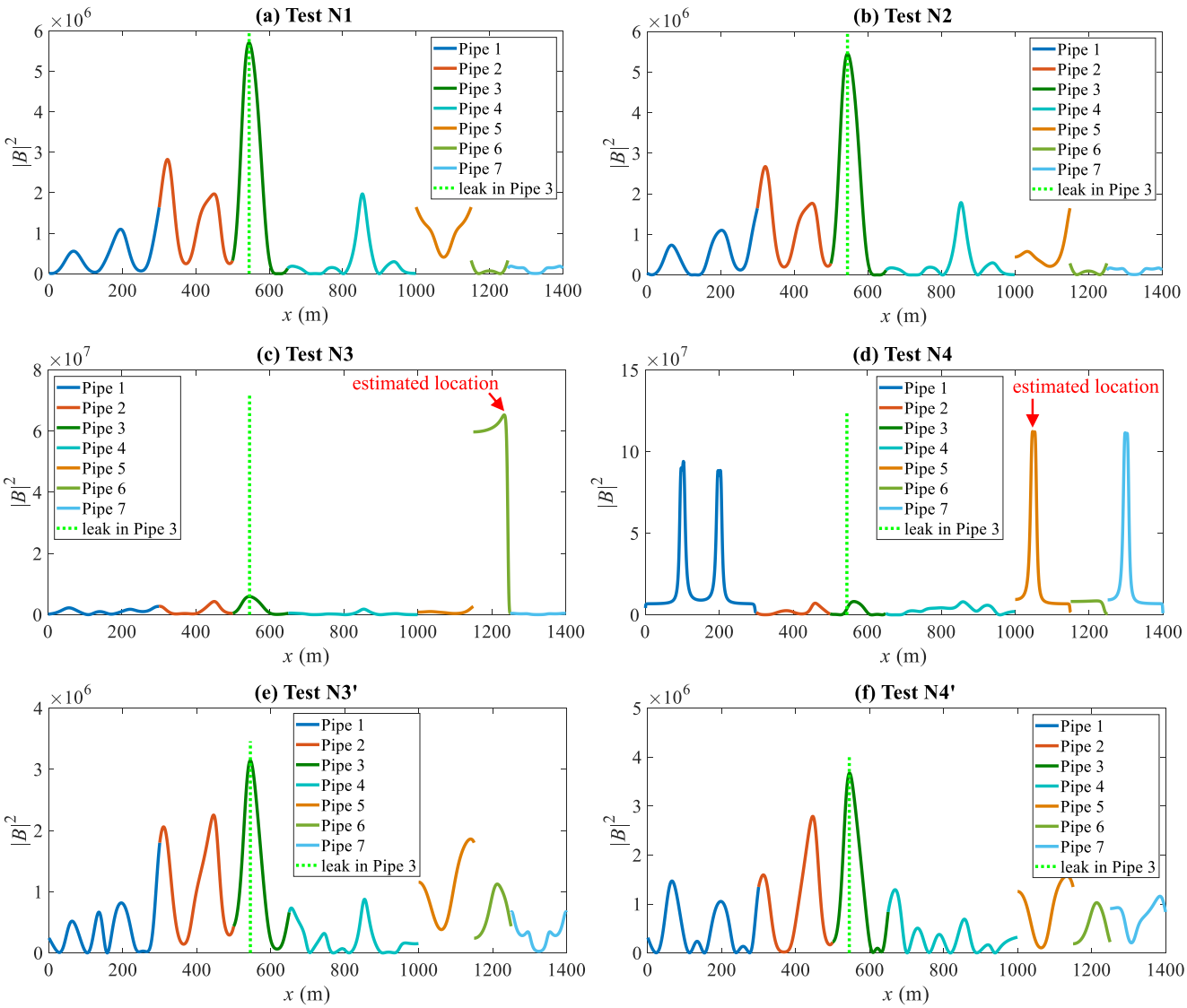

Figure 11. Localization results with different numbers of accessible boundaries: objective function for (a) Test N1, (b) Test N2, (c) Test N3, (d) Test N4, (e) Test N3′, and (f) Test N4′.

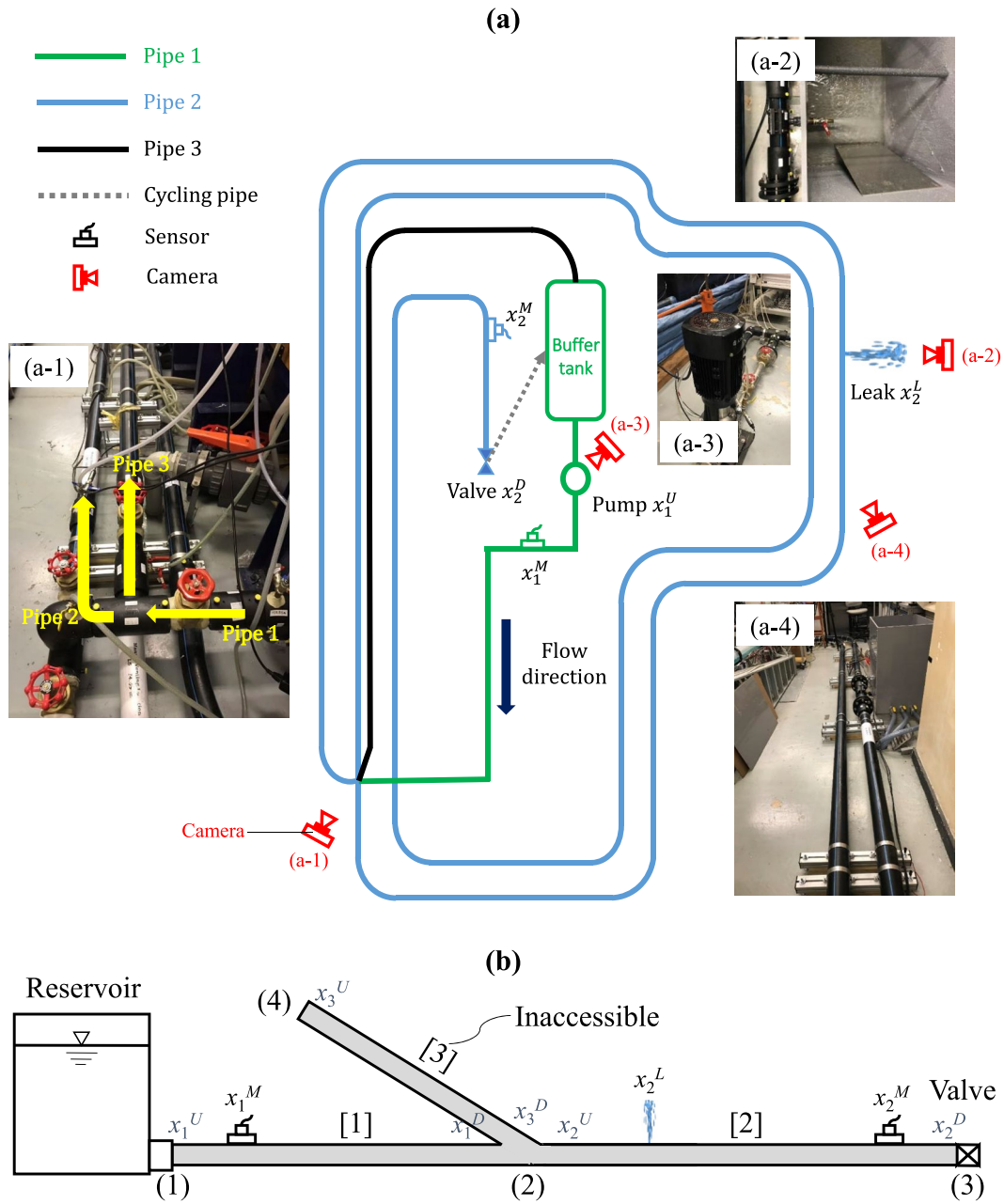

Figure 12. Tree network in the Water Resources Research Laboratory of HKUST (a) overall layout; and (b) simplified sketch.

Table 7
Parameters of HDPE Pipes in the Water Resources Research Laboratory of HKUST

$\nu = 0.43$	$\kappa = 2.1 \times 10^9$ Pa	$\rho = 10^3$ kg/m^3
$D = 79.2$ mm	$e = 5.4$ mm	$J_0 = 5.8 \times 10^{-10}$ Pa^{-1}
$J_1 = 1.96 \times 10^{-10}$ Pa^{-1}	$\tau_1 = 0.038$ s	$J_2 = 1.10 \times 10^{-10}$ Pa^{-1}
$\tau_2 = 0.6$ s	$J_3 = 9.05 \times 10^{-12}$ Pa^{-1}	$\tau_3 = 1.5$ s

Pressure waves are generated by a sudden and complete closure of the downstream valve at x_2^D within 0.06 s. Because Pipe [3] is assumed to be inaccessible, the pressure signals in Pipes [1] and [2] are collected for leak localization. The measured time domain pressure signals are plotted in Figure 13a, which are further transformed into the frequency domain to obtain their FRF signals in Figure 13b. It can be observed in Figure 13 that the measured signals are contaminated by noise and uncertainties. In the leak localization, the FRF signals are truncated at 5.5 Hz, that is, 0–5.5 Hz is used, because the signals become highly noisy after 5.5 Hz.

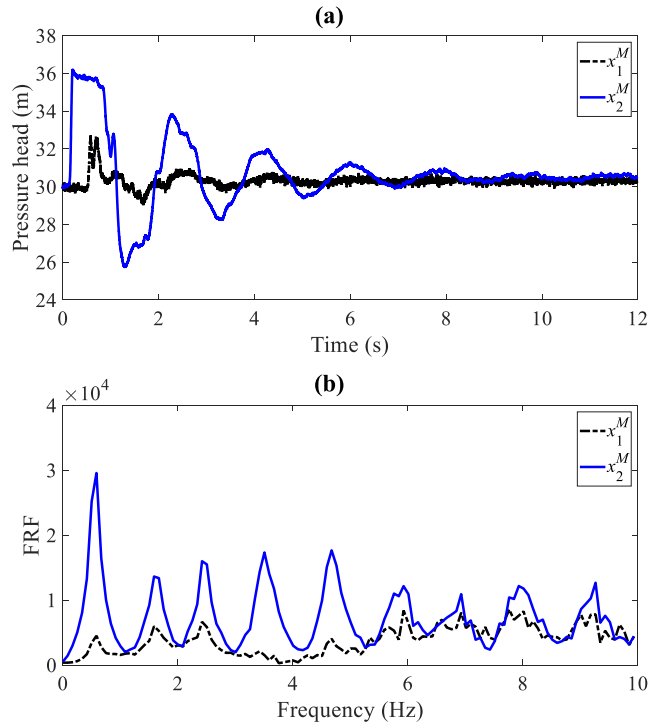

Figure 13. Pressure measurements by Sensors M1 and M2 in the: (a) time domain and (b) frequency domain.

Based on FRFs in Figure 13b, the MFP algorithm is implemented for leak localization by plotting the objective functions $|B|^2$ in Equation 40 of three pipes in Figure 14. The objective function $|B|^2$ has a global maximum value in Pipe [2] at 25.01 m away from the internal Node (2), which means the leak localization error is $|30 - 25.01| = 4.99$ m. This error is much lower than the diffraction limit $\lambda_{\min}/2 = a/(2f_{\max}) \approx 365/(2 \times 5.5) \approx 33$ m of the probing wave implying that the localization result is acceptable, where $f_{\max}$ = the maximum frequency of the probing wave.

Note that the validity of the proposed MFP algorithm with a modified model for leak localization is preliminarily confirmed by the experimental data from a previously published paper (Wang et al., 2021), where the prototype of the modified model in the present paper was developed. The detectability of leaks with different sizes by the proposed MFP algorithm was not systematically investigated, which is the main limitation of this section.

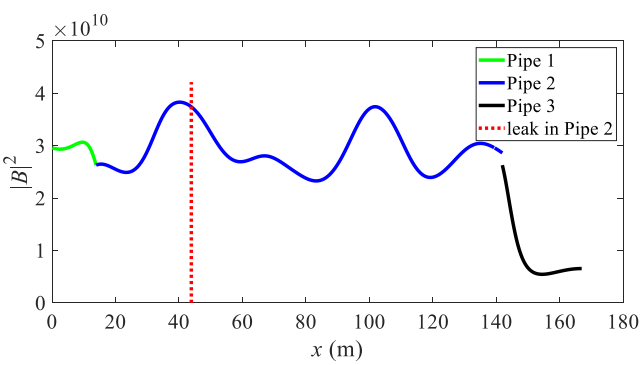

Figure 14. Leak localization result using experimental data.

6. Conclusions

This paper formulates a modified factorized wave model for tree networks, based on which the robust and efficient MFP method can be implemented for leak localization without the strict accessibility requirement of all external pipes. This is realized by linearizing and factorizing the point transfer matrices of external pipes based on the small leak approximation.

The validity of the modified MFP method is confirmed by numerical and laboratory experiments conducted in tree networks. Numerical experiments indicate that the modified algorithm uniquely and accurately localizes a single leak anywhere in tree networks. The ability to resolve two co-existing leaks separated larger than half the minimum probing wavelength is also demonstrated. Laboratory experiments show that the modified algorithm can successfully localize the leak in a tree network even though the measured pressure signals are contaminated by background noise.

Appendix A: Derivation of the Concrete Form of G in Equation 16

Equation 15 is carbon copied as

$$\begin{bmatrix} q\left(x_2^M\right) \\ h\left(x_2^M\right) \end{bmatrix} = \begin{bmatrix} q^{NL}\left(x_2^M\right) \\ h^{NL}\left(x_2^M\right) \end{bmatrix} + s_1^L \mathbf{F}^{NL}\left(x_2^U \to x_2^M\right) \mathbf{F}^{SL}\left(x_1^U \to x_1^L \to x_1^D\right) \begin{bmatrix} q\left(x_1^U\right) \\ h\left(x_1^U\right) \end{bmatrix} \tag{A1}$$

in which

$$\mathbf{F}^{NL}\left(x_2^U \to x_2^M\right) = \begin{bmatrix} \cosh(\mu_2 L_2) & -\frac{1}{Z_2}\sinh(\mu_2 L_2) \\ -Z_2\sinh(\mu_2 L_2) & \cosh(\mu_2 L_2) \end{bmatrix} \tag{A2}$$

$$\mathbf{F}^{SL}\left(x_1^U \to x_1^L \to x_1^D\right) = \sqrt{\frac{g}{2H_0^L}} \begin{bmatrix} Z_1\cosh\left[\mu_1\left(x_1^D - x_1^L\right)\right]\sinh\left[\mu_1\left(x_1^L - x_1^U\right)\right] & -\cosh\left[\mu_1\left(x_1^D - x_1^L\right)\right]\cosh\left[\mu_1\left(x_1^L - x_1^U\right)\right] \\ -Z_1^2\sinh\left[\mu_1\left(x_1^D - x_1^L\right)\right]\sinh\left[\mu_1\left(x_1^L - x_1^U\right)\right] & Z_1\sinh\left[\mu_1\left(x_1^D - x_1^L\right)\right]\cosh\left[\mu_1\left(x_1^L - x_1^U\right)\right] \end{bmatrix} \tag{A3}$$

where Z_p = impedance of Pipe [p]; and μ_p = propagation function μ of Pipe [p].

Substituting Equations A2 and A3 to Equation A1 and taking the second row gives Equation 16 as

$$h\left(x_2^M\right) = h^{NL}\left(x_2^M\right) + s_1^L G\left(x_2^M, x_1^L\right) \tag{A4}$$

where the concrete form of $G\left(x_2^M, x_1^L\right)$ is

$$\begin{aligned} G\left(x_2^M, x_1^L\right) = & \sqrt{\frac{g}{2H_0^L}} \{ -Z_1 Z_2 \sinh(\mu_2 L_2)\cosh\left[\mu_1\left(x_1^D - x_1^L\right)\right]\sinh\left[\mu_1\left(x_1^L - x_1^U\right)\right] q\left(x_1^U\right) \\ & - Z_1^2\cosh(\mu_2 L_2)\sinh\left[\mu_1\left(x_1^D - x_1^L\right)\right]\sinh\left[\mu_1\left(x_1^L - x_1^U\right)\right] q\left(x_1^U\right) \\ & + Z_2\sinh(\mu_2 L_2)\cosh\left[\mu_1\left(x_1^D - x_1^L\right)\right]\cosh\left[\mu_1\left(x_1^L - x_1^U\right)\right] h\left(x_1^U\right) \\ & + Z_1\cosh(\mu_2 L_2)\sinh\left[\mu_1\left(x_1^D - x_1^L\right)\right]\cosh\left[\mu_1\left(x_1^L - x_1^U\right)\right] h\left(x_1^U\right) \} \end{aligned} \tag{A5}$$

Appendix B: Point Matrix of a Non-Measured External Pipe

This section derives the point matrix of a non-measured external pipe bounded by a dead end. The point matrices of non-measured external pipes bounded by other common boundaries (e.g., a reservoir) can be derived following similar procedures.

Equations 1 and 2 of a non-measured external Pipe [p] without any leak can be written as

$$q\left(x_p^D\right) = F_{11}(L_p)\, q\left(x_p^U\right) + F_{12}(L_p)\, h\left(x_p^U\right) \tag{B1}$$

$$h\left(x_p^D\right) = F_{21}(L_p)\, q\left(x_p^U\right) + F_{22}(L_p)\, h\left(x_p^U\right) \tag{B2}$$

The mass and momentum equations across the internal Node (v^J) connected to the downstream end of Pipe [p] are

$$q\left(x^{JU}\right) = (-1)^{\alpha_1} q\left(x_p^D\right) + q\left(x^{JD}\right) \tag{B3}$$

$$h\left(x^{JU}\right) = h\left(x_p^D\right) = h\left(x^{JD}\right) \tag{B4}$$

where x^{JU} = coordinate of the pipe end in the mother pipe of Node (v^J); $q\left(x^{JD}\right) = \sum_{i=2}^{I_c} (-1)^{\alpha_i} q\left(x_i^{JD}\right)$ is the discharge summation of all child pipes (except Pipe [p]) infinitely approaching Node (v^J); and $h\left(x^{JD}\right) = h\left(x_i^{JD}\right)$ is the pressure head of child pipes ($i = 2, \ldots, I_c$) infinitely approaching Node (v^J).

The concrete form of the point matrix for the non-measured external Pipe $[p]$ depends on the specific boundary condition at x_p^U, a dead end gives

$$q\left(x_p^U\right) = 0 \tag{B5}$$

Substituting Equation B5 to Equations B1 and B2 gives

$$q\left(x_p^D\right) = \frac{F_{12}(L_p)}{F_{22}(L_p)} h\left(x_p^D\right) \tag{B6}$$

Substituting Equations B6 and B4 to Equation B3 gives

$$q\left(x^{JU}\right) = q\left(x^{JD}\right) + (-1)^{\alpha_1} \frac{F_{12}(L_p)}{F_{22}(L_p)} h\left(x^{JD}\right) \tag{B7}$$

Rewrite Equation B4 as

$$h\left(x^{JU}\right) = 0 \cdot q\left(x^{JD}\right) + h\left(x^{JD}\right) \tag{B8}$$

Equations B7 and B8 can be written in the matrix form as

$$\begin{bmatrix} q\left(x^{JU}\right) \\ h\left(x^{JU}\right) \end{bmatrix} = \begin{bmatrix} 1 & (-1)^{\alpha_1} \frac{F_{12}(L_p)}{F_{22}(L_p)} \\ 0 & 1 \end{bmatrix} \begin{bmatrix} q\left(x^{JD}\right) \\ h\left(x^{JD}\right) \end{bmatrix} \tag{B9}$$

Therefore, the point matrix of the non-measured external Pipe $[p]$ is

$$\mathbf{P}_b^{NL}\left(x^{JD} \to x^{JU}\right) = \begin{bmatrix} 1 & (-1)^{\alpha_1} \frac{F_{12}(L_p)}{F_{22}(L_p)} \\ 0 & 1 \end{bmatrix} \tag{B10}$$

Appendix C: Amplification Coefficients of the Measurement Noise

In Figure 2, the pressure head of the upstream reservoir is assumed to be constant, which gives the boundary condition $h\left(x_1^U\right) = 0$; thus, it has no measurement noise. Whereas the discharge of the reservoir is computed from pressure measurement of Sensor M1 (Che et al., 2022), which is contaminated by noise $\delta q(\omega_j)$. Therefore, the contaminated $\tilde{q}^{NL}$ and $\tilde{h}^{NL}$ at frequency ω_j can be computed as

$$\begin{bmatrix} \tilde{q}^{NL}\left(x_2^M, \omega_j\right) \\ \tilde{h}^{NL}\left(x_2^M, \omega_j\right) \end{bmatrix} = \mathbf{F}^{NL}\left(x_2^U \to x_2^M\right) \mathbf{P}_b^{NL}\left(x_1^D \to x_2^U\right) \mathbf{F}^{NL}\left(x_1^U \to x_1^D\right) \begin{bmatrix} q\left(x_1^U, \omega_j\right) + \delta q(\omega_j) \\ h\left(x_1^U, \omega_j\right) \end{bmatrix} \tag{C1}$$

Substituting field and point matrix elements to Equation C1 and taking the second row give

$$\begin{aligned} \tilde{h}^{NL}\left(x_2^M, \omega_j\right) = h^{NL}\left(x_2^M, \omega_j\right) & \\ + \underbrace{F_{21}(L_2, \omega_j)\, F_{11}(L_1, \omega_j)}_{C_1(\omega_j)} \delta q(\omega_j) & \\ + \underbrace{F_{22}(L_2, \omega_j)\, F_{21}(L_1, \omega_j)}_{C_2(\omega_j)} \delta q(\omega_j) & \\ + \underbrace{F_{21}(L_2, \omega_j)\, F_{21}(L_1, \omega_j) \frac{F_{12}(L_3, \omega_j)}{F_{22}(L_3, \omega_j)}}_{C_3(\omega_j)} \delta q(\omega_j) & \end{aligned} \tag{C2}$$

Note that the amplification coefficients of the measurement noise for a general tree network can be derived following similar procedures.

Appendix D: Estimating Unknown Leak Location and Size

The objective of this appendix is to estimate the unknown leak location x_p^L and size s_p^L by the filtered measurement $\Delta\mathbf{h}_f$. The basic idea of the MFP method (Wang & Ghidaoui, 2018b) is to adjust a J_f-dimensional unit vector $\mathbf{w}$ (i.e., $|\mathbf{w}| = 1$), by changing the assumed leak location, to have the same direction with $\Delta\mathbf{h}_f$. The inner product of the unit vector $\mathbf{w}$ and $\Delta\mathbf{h}_f$ is

$$B \equiv < \mathbf{w}, \Delta\mathbf{h}_f > = \mathbf{w}^{\mathrm{H}}\Delta\mathbf{h}_f \in \mathbb{C} \tag{D1}$$

The optimal unit vector $\hat{\mathbf{w}}$ is obtained by maximizing the following objective function

$$|B|^2 = |\mathbf{w}^{\mathrm{H}}\Delta\mathbf{h}_f|^2 = \mathbf{w}^{\mathrm{H}}\Delta\mathbf{h}_f\Delta\mathbf{h}_f^{\mathrm{H}}\mathbf{w} \tag{D2}$$

Substituting Equation 39 to Equation D2 and maximizing its expectation give the optimal unit vector $\hat{\mathbf{w}}$

$$\hat{\mathbf{w}} = \arg\max_{\mathbf{w}} \mathbb{E}\left(|B|^2\right) = \arg\max_{\mathbf{w}} \left[\left(s_p^L\right)^2 \mathbf{w}^{\mathrm{H}}\mathbf{G}_f\mathbf{G}_f^{\mathrm{H}}\mathbf{w} + \sigma^2\right] = \arg\max_{\mathbf{w}} \left(\mathbf{w}^{\mathrm{H}}\mathbf{G}_f\mathbf{G}_f^{\mathrm{H}}\mathbf{w}\right) = \pm\frac{\mathbf{G}_f}{\sqrt{\mathbf{G}_f^{\mathrm{H}}\mathbf{G}_f}} \tag{D3}$$

It turns out that the optimal $\hat{\mathbf{w}}$ is a unit vector parallel to $\mathbf{G}_f$. Thus, the optimal leak location can be estimated by substituting Equation D3 to Equation D2

$$\hat{x_p^L} = \arg\max_{x_p^L} |B|^2 = \arg\max_{x_p^L} \frac{\Delta\mathbf{h}_f^{\mathrm{H}}\mathbf{G}_f\left(x_p^L\right)\mathbf{G}_f^{\mathrm{H}}\left(x_p^L\right)\Delta\mathbf{h}_f}{\mathbf{G}_f^{\mathrm{H}}\left(x_p^L\right)\mathbf{G}_f\left(x_p^L\right)} \tag{D4}$$

Once the optimal leak location is determined, the optimal leak size can be estimated by the maximum likelihood estimation (Che et al., 2022; Wang & Ghidaoui, 2018b) as

$$\hat{s_p^L} = \frac{\mathbf{G}_f^{\mathrm{H}}\left(\hat{x_p^L}\right)\Delta\mathbf{h}_f}{\mathbf{G}_f^{\mathrm{H}}\left(\hat{x_p^L}\right)\mathbf{G}_f\left(\hat{x_p^L}\right)} \tag{D5}$$

Notation

A	pipe cross-sectional area
a	wave speed
C	amplification coefficient of measurement noise
D	pipe diameter
E	pipe set
$\mathbf{F}$	field transfer matrix
$\mathbf{F}^{SL}$	scattering matrix due to leak
f_{DW}	Darcy–Weisbach friction factor
h	pressure head perturbation in the frequency domain
h^{NL}	pressure head perturbation in the frequency domain of the leak-free case
$\mathbf{n}$	measurement noise
$\mathbf{P}$	point transfer matrix
$\mathbf{P}_b$	point transfer matrix of the non-measured external pipe
p^L	ID number of the leaky pipe
Q_0	steady state discharge
q	discharge perturbation in the frequency domain
s_p^L	leak size
V	node set
x_p^D	local coordinate of the downstream end of Pipe $[p]$

x_p^M	local coordinate of the pressure sensor in Pipe $[p]$
x_p^U	local coordinate of the upstream end of Pipe $[p]$
x_p^L	leak location
Z	characteristic impedance
$\mathbf{\Delta h}$	leak induced pressure difference
ω	angular frequency

Data Availability Statement

The numerical and experimental data used for leak localization in this paper are available at Personal Web: https://chetongchuan.wixsite.com/hohai/code, or MATLAB Drive: https://drive.matlab.com/sharing/36e4fb1e-5449-4dd8-9692-b538c2d75d6a/.

Acknowledgments
This research was supported by research grants from the National Natural Science Foundation of China (Grants 52209084, 1839008, and 52005016) and the Hong Kong Research Grants Council (Grant 15200719). The authors would like to thank Prof. Mohamed S. Ghidaoui for several constructive discussions on the small leak approximation and thank Dr. G. Adriana Camino for the well-designed transient experiments in HKUST during the Theme-based RGC project on Smart Urban Water Supply Systems (T21-602/15-R).

References

Alawadhi, A., Boso, F., & Tartakovsky, D. M. (2018). Method of distributions for water hammer equations with uncertain parameters. *Water Resources Research*, *54*(11), 9398–9411. https://doi.org/10.1029/2018wr023383

Alawadhi, A., & Tartakovsky, D. M. (2020). Bayesian update and method of distributions: Application to leak detection in transmission mains. *Water Resources Research*, *56*(2), e2019WR025879. https://doi.org/10.1029/2019wr025879

Beck, S. B., Curren, M. D., Sims, N. D., & Stanway, R. (2005). Pipeline network features and leak detection by cross-correlation analysis of reflected waves. *Journal of Hydraulic Engineering*, *131*(8), 715–723. https://doi.org/10.1061/(asce)0733-9429(2005)131:8(715)

Bohorquez, J., Alexander, B., Simpson, A. R., & Lambert, M. F. (2020). Leak detection and topology identification in pipelines using fluid transients and artificial neural networks. *Journal of Water Resources Planning and Management*, *146*(6), 04020040. https://doi.org/10.1061/(asce)wr.1943-5452.0001187

Bohorquez, J., Lambert, M. F., Alexander, B., Simpson, A. R., & Abbott, D. (2022). Stochastic resonance enhancement for leak detection in pipelines using fluid transients and convolutional neural networks. *Journal of Water Resources Planning and Management*, *148*(3), 04022001. https://doi.org/10.1061/(asce)wr.1943-5452.0001504

Brunone, B. (1999). Transient test-based technique for leak detection in outfall pipes. *Journal of Water Resources Planning and Management*, *125*(5), 302–306. https://doi.org/10.1061/(asce)0733-9496(1999)125:5(302)

Brunone, B., Maietta, F., Capponi, C., Keramat, A., & Meniconi, S. (2022). A review of physical experiments for leak detection in water pipes through transient tests for addressing future research. *Journal of Hydraulic Research*, *60*(6), 1–13. https://doi.org/10.1080/00221686.2022.2067086

Capponi, C., Ferrante, M., Zecchin, A. C., & Gong, J. (2017). Leak detection in a branched system by inverse transient analysis with the admittance matrix method. *Water Resources Management*, *31*(13), 4075–4089. https://doi.org/10.1007/s11269-017-1730-6

Capponi, C., Meniconi, S., Lee, P. J., Brunone, B., & Cifrodelli, M. (2020). Time-domain analysis of laboratory experiments on the transient pressure damping in a leaky polymeric pipe. *Water Resources Management*, *34*(2), 501–514. https://doi.org/10.1007/s11269-019-02454-x

Chaudhry, M. H. (2014). *Applied hydraulic transients*. Springer.

Che, T.-C., Duan, H.-F., & Lee, P. J. (2021). Transient wave-based methods for anomaly detection in fluid pipes: A review. *Mechanical Systems and Signal Processing*, *160*, 107874. https://doi.org/10.1016/j.ymssp.2021.107874

Che, T.-C., Wang, X., & Ghidaoui, M. S. (2022). Leak localization in looped pipe networks based on a factorized transient wave model: Theoretical framework. *Water Resources Research*, *58*(4), e2021WR031364. https://doi.org/10.1029/2021wr031364

Colombo, A. F., Lee, P., & Karney, B. W. (2009). A selective literature review of transient-based leak detection methods. *Journal of Hydro-Environment Research*, *2*(4), 212–227. https://doi.org/10.1016/j.jher.2009.02.003

Covas, D., & Ramos, H. (2010). Case studies of leak detection and location in water pipe systems by inverse transient analysis. *Journal of Water Resources Planning and Management*, *136*(2), 248–257. https://doi.org/10.1061/(asce)0733-9496(2010)136:2(248)

Covas, D., Stoianov, I., Mano, J. F., Ramos, H., Graham, N., & Maksimovic, C. (2005). The dynamic effect of pipe-wall viscoelasticity in hydraulic transients. Part II—Model development, calibration and verification. *Journal of Hydraulic Research*, *43*(1), 56–70. https://doi.org/10.1080/00221680509500111

Duan, H.-F. (2017). Transient frequency response based leak detection in water supply pipeline systems with branched and looped junctions. *Journal of Hydroinformatics*, *19*(1), 17–30. https://doi.org/10.2166/hydro.2016.008

Duan, H.-F., Pan, B., Wang, M., Chen, L., Zheng, F., & Zhang, Y. (2020). State-of-the-art review on the transient flow modeling and utilization for urban water supply system (UWSS) management. *Journal of Water Supply: Research and Technology—Aqua*, *69*(8), 858–893. https://doi.org/10.2166/aqua.2020.048

Fernandes, C., & Karney, B. W. (2004). Modelling the advection equation under water hammer conditions. *Urban Water Journal*, *1*(2), 97–112. https://doi.org/10.1080/15730620412331290038

Ferrante, M., & Brunone, B. (2003). Pipe system diagnosis and leak detection by unsteady-state tests. 2. Wavelet analysis. *Advances in Water Resources*, *26*(1), 107–116. https://doi.org/10.1016/s0309-1708(02)00102-1

Ferrante, M., Brunone, B., & Meniconi, S. (2007). Wavelets for the analysis of transient pressure signals for leak detection. *Journal of Hydraulic Engineering*, *133*(11), 1274–1282. https://doi.org/10.1061/(asce)0733-9429(2007)133:11(1274)

Ferrante, M., Brunone, B., & Meniconi, S. (2009). Leak detection in branched pipe systems coupling wavelet analysis and a Lagrangian model. *Journal of Water Supply: Research and Technology—Aqua*, *58*(2), 95–106. https://doi.org/10.2166/aqua.2009.022

Gong, J., Lambert, M. F., Simpson, A. R., & Zecchin, A. C. (2013). Single-event leak detection in pipeline using first three resonant responses. *Journal of Hydraulic Engineering*, *139*(6), 645–655. https://doi.org/10.1061/(asce)hy.1943-7900.0000720

Hamilton, S., & Charalambous, B. (2013). *Leak detection: Technology and implementation*. IWA Publishing.

Huang, Y., Zheng, F., Kapelan, Z., Savic, D., Duan, H.-F., & Zhang, Q. (2020). Efficient leak localization in water distribution systems using multistage optimal valve operations and smart demand metering. *Water Resources Research*, *56*(10), e2020WR028285. https://doi.org/10.1029/2020wr028285

Kapelan, Z. S., Savic, D. A., & Walters, G. A. (2003). A hybrid inverse transient model for leakage detection and roughness calibration in pipe networks. *Journal of Hydraulic Research*, *41*(5), 481–492. https://doi.org/10.1080/00221680309499993

Karney, B. W., & McInnis, D. (1992). Efficient calculation of transient flow in simple pipe networks. *Journal of Hydraulic Engineering*, *118*(7), 1014–1030. https://doi.org/10.1061/(asce)0733-9429(1992)118:7(1014)

Kashima, A., Lee, P. J., Ghidaoui, M. S., & Davidson, M. (2013). Experimental verification of the kinetic differential pressure method for flow measurements. *Journal of Hydraulic Research*, *51*(6), 634–644. https://doi.org/10.1080/00221686.2013.818583

Keramat, A., Karney, B., Ghidaoui, M. S., & Wang, X. (2021). Transient-based leak detection in the frequency domain considering fluid–structure interaction and viscoelasticity. *Mechanical Systems and Signal Processing*, *153*, 107500. https://doi.org/10.1016/j.ymssp.2020.107500

Kim, S. (2016). Impedance method for abnormality detection of a branched pipeline system. *Water Resources Management*, *30*(3), 1101–1115. https://doi.org/10.1007/s11269-015-1213-6

Kim, S., Zecchin, A., & Choi, L. (2014). Diagnosis of a pipeline system for transient flow in low Reynolds number with impedance method. *Journal of Hydraulic Engineering*, *140*(12), 04014063. https://doi.org/10.1061/(asce)hy.1943-7900.0000945

Lee, P. J., Lambert, M. F., Simpson, A. R., Vitkovsky, J. P., & Liggett, J. (2006). Experimental verification of the frequency response method for pipeline leak detection. *Journal of Hydraulic Research*, *44*(5), 693–707. https://doi.org/10.1080/00221686.2006.9521718

Lee, P. J., Vitkovsky, J. P., Lambert, M. F., Simpson, A. R., & Liggett, J. (2007). Leak location in pipelines using the impulse response function. *Journal of Hydraulic Research*, *45*(5), 643–652. https://doi.org/10.1080/00221686.2007.9521800

Liemberger, R., & Wyatt, A. (2019). Quantifying the global non-revenue water problem. *Water Supply*, *19*(3), 831–837. https://doi.org/10.2166/ws.2018.129

Liggett, J. A., & Chen, L.-C. (1994). Inverse transient analysis in pipe networks. *Journal of Hydraulic Engineering*, *120*(8), 934–955. https://doi.org/10.1061/(asce)0733-9429(1994)120:8(934)

Lin, J., Wang, X., & Ghidaoui, M. S. (2021). Multi-sensor fusion for transient-based pipeline leak localization in the Dempster-Shafer evidence framework. *Water Resources Research*, *57*(9), e2021WR029926. https://doi.org/10.1029/2021wr029926

Meniconi, S., Brunone, B., Ferrante, M., Capponi, C., Carrettini, C., Chiesa, C., et al. (2015). Anomaly pre-localization in distribution–transmission mains by pump trip: Preliminary field tests in the Milan pipe system. *Journal of Hydroinformatics*, *17*(3), 377–389. https://doi.org/10.2166/hydro.2014.038

Meniconi, S., Capponi, C., Frisinghelli, M., & Brunone, B. (2021). Leak detection in a real transmission main through transient tests: Deeds and misdeeds. *Water Resources Research*, *57*(3), e2020WR027838. https://doi.org/10.1029/2020wr027838

Meniconi, S., Cifrodelli, M., Capponi, C., Duan, H.-F., & Brunone, B. (2021). Transient response analysis of branched pipe systems toward a reliable skeletonization. *Journal of Water Resources Planning and Management*, *147*(2), 04020109. https://doi.org/10.1061/(asce)wr.1943-5452.0001319

Nguyen, S. T. N., Gong, J., Lambert, M. F., Zecchin, A. C., & Simpson, A. R. (2018). Least squares deconvolution for leak detection with a pseudo random binary sequence excitation. *Mechanical Systems and Signal Processing*, *99*, 846–858. https://doi.org/10.1016/j.ymssp.2017.07.003

Nixon, W., Ghidaoui, M. S., & Kolyshkin, A. A. (2006). Range of validity of the transient damping leakage detection method. *Journal of Hydraulic Engineering*, *132*(9), 944–957. https://doi.org/10.1061/(asce)0733-9429(2006)132:9(944)

Pan, B., Capponi, C., Meniconi, S., Brunone, B., & Duan, H.-F. (2022). Efficient leak detection in single and branched polymeric pipeline systems by transient wave analysis. *Mechanical Systems and Signal Processing*, *162*, 108084. https://doi.org/10.1016/j.ymssp.2021.108084

Qi, Z., Zheng, F., Guo, D., Zhang, T., Shao, Y., Yu, T., et al. (2018). A comprehensive framework to evaluate hydraulic and water quality impacts of pipe breaks on water distribution systems. *Water Resources Research*, *54*(10), 8174–8195. https://doi.org/10.1029/2018wr022736

Wang, X. (2021). Uncertainty quantification and global sensitivity analysis for transient wave propagation in pressurized pipes. *Water Resources Research*, *57*(4), e2020WR028975. https://doi.org/10.1029/2020wr028975

Wang, X., Camino, G. A., Che, T.-C., & Ghidaoui, M. S. (2021). Factorized wave propagation model in tree-type pipe networks and its application to leak localization. *Mechanical Systems and Signal Processing*, *147*, 107116. https://doi.org/10.1016/j.ymssp.2020.107116

Wang, X., & Ghidaoui, M. S. (2018a). Identification of multiple leaks in pipeline: Linearized model, maximum likelihood, and super-resolution localization. *Mechanical Systems and Signal Processing*, *107*, 529–548. https://doi.org/10.1016/j.ymssp.2018.01.042

Wang, X., & Ghidaoui, M. S. (2018b). Pipeline leak detection using the matched-field processing method. *Journal of Hydraulic Engineering*, *144*(6), 04018030. https://doi.org/10.1061/(asce)hy.1943-7900.0001476

Wang, X., Lambert, M. F., Simpson, A. R., Liggett, J. A., & Vitkovsky, J. P. (2002). Leak detection in pipelines using the damping of fluid transients. *Journal of Hydraulic Engineering*, *128*(7), 697–711. https://doi.org/10.1061/(asce)0733-9429(2002)128:7(697)

Waqar, M., Louati, M., Wang, X., & Ghidaoui, M. S. (2021). Model-free matched field processing for condition assessment of pressurized pipes. *Journal of Water Resources Planning and Management*, *147*(10), 04021066. https://doi.org/10.1061/(asce)wr.1943-5452.0001447

Zecchin, A., Lambert, M., Simpson, A., & White, L. (2014). Parameter identification in pipeline networks: Transient-based expectation-maximization approach for systems containing unknown boundary conditions. *Journal of Hydraulic Engineering*, *140*(6), 04014020. https://doi.org/10.1061/(asce)hy.1943-7900.0000849

Zeng, W., Gong, J., Simpson, A. R., Cazzolato, B. S., Zecchin, A. C., & Lambert, M. F. (2020). Paired-IRF method for detecting leaks in pipe networks. *Journal of Water Resources Planning and Management*, *146*(5), 04020021. https://doi.org/10.1061/(asce)wr.1943-5452.0001193